

Chapter 3 Naringin: a naturally occurring flavonoid as a photoinitiator for 3D printed electro-active actuator

3.1 Preface

Thanks to their versatile photoinitiation abilities, natural flavone derivatives (i.e., quercetin and morin) based photoinitiating systems have potential for diverse materials in industries, for example, Bis-GMA/TEGDMA blend for dental restoration, etc.¹ However, the used monomer systems are all hydrophobic. In contrast, hydrophilic hydrogels have been widely employed in advanced applications, for example, cell scaffolds, actuators, etc.^{2,3} Additionally, considering the light intensity of the used LEDs (80-110 mW cm⁻²) for quercetin and morin, their photoinitiation abilities are insufficient to be employed in 3D resins for DLP 3D printing. Therefore, to be involved in water-favorable 3D resins, hydrophilic natural photoinitiators are imperative. The deprotonated hydroxyl group exhibited great water solubilities; therefore, natural multi-hydroxyl substituted flavones are promising photoinitiator candidates for water-favorable resins. In the present chapter, a multi-hydroxyl substituted flavone derivative, naringin extracted from citrus, has been comprehensively investigated as water-favorable formulas under the irradiation of visible light. This chapter aims to: a) validate its photoinitiation abilities in water-favorable resins (i.e., poly(ethylene glycol) diacrylate resins); b) demonstrate the composition of the naringin based 3D resins for high-fidelity 3D printing; c) optimize the naringin based 3D resin composition to achieve a 3D printed soft robotics actuated by an electric field.

3.2 Abstract

The utilization of actuator in soft robotics has attracted significant attention. Nonetheless, the manufacture of these actuators heavily relies on a modelling process, limiting their customization potential. Photopolymerization-based 3D printing has emerged as a promising solution to address this limitation. However, challenges persist with the commonly used photoinitiators in 3D resins, encompassing environmental concerns, sensitivity to visible light, and water solubility. Herein, we present a novel approach utilizing a naturally occurring plant extract, naringin, known for its safety profile and sensitivity to visible light. We develop an exceptional photoinitiating system based on naringin, showcasing remarkable abilities in initiating free radical photopolymerization. Leveraging this advancement, we successfully 3D printed a figurine with precise surface texture. Furthermore, we optimize the 3D resin formula by introducing an electro-sensitive component, sodium acrylate, aiming to create electro-stimulated actuators. Beyond its electro-sensitivity, the incorporation of sodium acrylate

significantly influences the photopolymerization performance and polymer deformation. Through meticulous formulation, we successfully fabricate actuators that display actuation behavior when subjected to an applied electric field. This study demonstrates a novel pathway for developing customizable actuators in soft robotics, addressing key challenges in their production while showcasing potential applications in responsive and adaptable systems.

3.3 Introduction

Actuators have gained great interest due to their response to environmental stimuli, enabling programmed physical movement upon activation.^{4, 5} With carefully designed configurations, diverse shape transformations to actuators, for instance, roll, wave, helix, etc., could be achieved.⁶ As their development has progressed, these actuators have been tailored to respond to specific stimuli like moisture, heat, light, and electricity, leading to a broad spectrum of applications.^{5, 7-22} For instance, drawing inspiration from soft-bodied organisms, a fast-moving fish robotic device with an actuator was engineered to swim at 13.5 cm s^{-1} upon electrostimulation (10 kV and 5 Hz).²³ Thanks to its response to electricity, fabricated actuator can operate in harsh environments. However, the actuator was produced via a molding process. Even though molding is a fast and cost-effective method, it cannot afford multi-material products and flexible production.² In contrast, photopolymerization-based 3D printing offers superior precision in creating intricate structures,² as seen in successfully 3D printing artificial cilia with robust actuation under UV irradiation.²² Despite the advantages of light-based 3D printing,²⁴ ongoing development of 3D resin remains crucial to mitigate potential safety and environmental concerns associated with photoinitiator migration.

Photopolymerization is the fundamental technology for 3D printing with light, and various 3D resins have been developed.²⁵ However, few of the developed photocurable formulas meet stringent safety and environmental protection standards. To address these challenges, considerable inherently biocompatible materials (e.g., poly(vinyl alcohol) (PVA), poly(ethylene glycol) (PEG), etc.) have been modified with photocurable functional groups (e.g., methacrylate or acrylate), and the developed photocurable polymers have been employed to safety-dependent photopolymer based applications such as bioprinting.²⁶ However, the safety of the photoinitiators used in these formulas remained uncertain, evident in cytotoxicity displayed by certain photoinitiators like phenylbis(2,4,6-trimethylbenzoyl)phosphine oxide (BAPO) used in the as aforementioned artificial cilia.^{22, 27} Even though only a trace amount of photoinitiators exist in 3D resin, their safety should still be considered. In contrast, the photoinitiators, 2-hydroxy-1-(4-(2-hydroxyethoxy)phenyl)-2-methyl-1-propanone (Irgacure 2959) and lithium phenyl-2,4,6-trimethylbenzoylphosphinate (LAP), involved in the fabrication

of biomaterials demonstrated both excellent biocompatibilities and water solubilities.²⁸ However, Irgacure 2959 cannot be included in 3D resins as it has little light absorption at wavelengths longer than 370 nm.²⁸ Unlike Irgacure 2959, LAP can afford a successful photopolymerization-based 3D printing, thanks to its good absorption at 365 nm and 405 nm. Typically, LAP has been employed in a high-resolution 3D bioprinting of a 50- μm scaffold seeded high density cells which mostly impeded the 3D printing resolution.²⁹ This state-of-the-art facilitates the development of a vascularized fully-functioned tissues or organs via 3D bioprinting. However, both Irgacure 2959 and LAP are synthetic photoinitiators, and their synthesis process may produce chemical pollutant. Therefore, a reliable source of photoinitiators is essential to prevent potential environmental concerns. Nature offers a repertoire of biocompatible photoinitiators³⁰ such as flavone derivatives, curcumin, chlorophyll a, riboflavin, beta-carotene, etc. demonstrating efficient photoinitiation abilities³¹⁻³⁶ under diverse irradiation from UV to red lights. Furthermore, most of them have been involved in safety-dependent applications (e.g., microneedles, antibacterials coatings, bone regeneration, etc.).^{35, 37, 38} Beta-carotene photoinitiated antibacterial coatings are of low water solubility. With the help of eugenol, the resulting beta-carotene photoinitiated hydrophobic antibacterial coating exhibited an 80% reduction in *E. coli* count.³⁵ In contrast, riboflavin photoinitiated microneedles and scaffold are water-rich hydrogels. Specifically, the riboflavin photoinitiated microneedles demonstrated evident transdermal drug delivery, and the 3D printed scaffold undertook active cell proliferation and resulted in complete biodegradation in 75 days.^{37, 38} As a result, riboflavin is favorable as a photoinitiator, as its migration would cause neither environmental nor health impact. However, the demands of either high light intensity (2100 mW cm⁻²) or additional post thermal curing (80 °C) for riboflavin photoinitiation significantly compromised its application scope. Therefore, it is desirable to further explore highly efficient naturally occurring photoinitiators with biocompatibility, excellent photoinitiation ability, and water solubility.

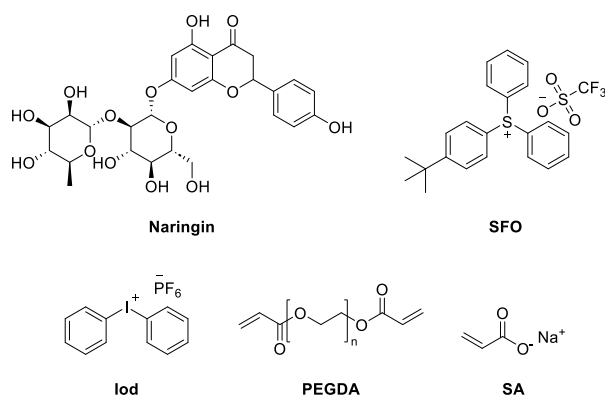
The present work introduced a plant extract, naringin, which can meet the abovementioned requirements as a favorable photoinitiator. Naringin is extracted from citrus fruits (e.g., grapefruit, etc.) and demonstrates strong anti-inflammatory and antioxidant activities.³⁹⁻⁴¹ Given its natural and edible origin, naringin emerges as a safe and non-toxic photoinitiator candidate. Owing to its multiple hydroxyl groups, naringin is a water-favorable compound, and the addition of alkali could facilitate its water solubility via the dissociation of hydrogen. Therefore, the concentration of alkali was investigated to achieve the augmented photoinitiation ability of naringin. The photoinitiation abilities were evaluated using a real-time Fourier-transform infrared spectroscopy (RT-FTIR). The mechanism during the photoreaction

of the developed photoinitiating system was studied by light absorption property and steady-state photolysis using an ultraviolet-visible (UV-vis) spectrophotometer, as well as the characterization of the generated free radicals using electron paramagnetic resonance spin trapping (EPR-ST) technique. To successfully fabricate a functional electro-stimulated actuator, the electro-active monomer, sodium acrylate (SA), was included for the production of the photopolymer, and the in-situ photorheology experiments and three-point bending tests were carried out with corresponding formulas. Thanks to the negatively charged carboxyl groups of SA, the produced photopolymer could move in line with the electricity flow. This conceptual design was validated in a continuous electric field. Consequently, a hand-like tool and a hook-like tool were successfully 3D printed, and the relevant electro-stimulated actuation behavior was observed.

3.4 Experimental

3.4.1 Materials

Naringin, diphenyliodonium hexafluorophosphate (Iod), (4-*tert*-butylphenyl)diphenylsulfonium triflate (SFO), poly(ethylene glycol) diacrylate (PEGDA) M_n 700 ($\rho = 1.12$ g mL⁻¹), sodium acrylate (SA), and phenyl-*N*-*tert*-butylnitron (PBN) were obtained from Sigma-Aldrich and used as delivered. The chemical structures of mentioned compounds are summarized in Scheme 3.1.



Scheme 3.1. Chemical structures of naringin, additives (SFO and Iod) of photoinitiating systems, and monomer/oligomers (PEGDA and SA).

3.4.2 Steady-state photolysis

The ultraviolet-visible light (UV-vis) absorption of naringin dissolved in deionized (DI) water or diverse concentrations of aqueous solutions of NaOH were measured on Varian Cary 50 Bio

UV-visible (UV-vis) spectrophotometer (Agilent Technologies). As to the steady-state photolysis experiment, the solution of naringin in aqueous 500 mM NaOH in the presence of Iod was irradiated using the LED@400 nm (6.4 mW cm⁻²). The light absorption profiles were recorded by the UV-vis spectrophotometer at different exposure time.

3.4.3 Electron Paramagnetic Resonance Spin Trapping (EPR-ST)

EPR-ST experiments were carried out in ambient condition on a Bruker E500 spectrometer equipped with a Bruker ER4122 SHQ resonator, as previously reported.³¹ Briefly, the tert-butylbenzene solution of naringin/Iod was loaded into standard X-band EPR tubes of 2.8 mm i.d.. The radicals were generated in a nitrogen atmosphere upon exposure to LED@400 nm and trapped by phenyl-*N*-tert-butyl nitron (PBN). The PBN/radical adducts were characterized by hyperfine splitting constants. The simulation was processed via the WINSIM application.

3.4.4 Photopolymerization kinetics

The photoinitiation ability of naringin was investigated using INVENIO®R, Fourier-transform infrared spectroscopy (FTIR) from Bruker, as previously reported.⁴² Briefly, to monitor the progress of the photopolymerization under the light irradiation, the samples were placed between two polypropylene films, avoiding oxygen diffusion. The double bond conversions of PEGDA/DI water blends were calculated by $D.C. = \left(1 - \frac{\int O.D.d\tilde{\nu}|_{t=t}}{\int O.D.d\tilde{\nu}|_{t=0}}\right) \times 100\%$. (O.D.: absorbance; $\tilde{\nu}$: wavenumber.), following the decrease of the acrylate C-H bond in-plane bending absorbance at 1414 cm⁻¹.⁴³⁻⁴⁵

3.4.5 Crosslinking network characteristics

The swelling behavior of the crosslinked polymeric materials were estimated via Flory-Rehner theory as the function of weight of relaxed ($M_{relaxed}$), swollen ($M_{swollen}$), and dry (M_{dry}).⁴⁶⁻⁵⁰ From the variables, the mesh sizes were quantified as the characteristic ratio of polymer ($C_N = 4$), the molecular weight of the repeat units ($M_r = 44$), the polymer volume fraction in swelling state ($v_{2,s}$), the molecular weight between the crosslinks ($\overline{M_c}$), and the bond length of the polymer backbone ($l = 1.54 \text{ \AA}$).

$$\xi = v_{2,s}^{-1/3} \left(\frac{2C_N \overline{M_c}}{M_r} \right)^{1/2} l$$

The equilibrium swelling equation was used to determine the $\overline{M_c}$,

$$\frac{1}{\overline{M}_C} = \frac{2}{\overline{M}_N} - \frac{(\overline{v}/V_1)[\ln(1 - v_{2,s}) + v_{2,s} + \chi_1 v_{2,s}^2]}{v_{2,r} \left[\left(\frac{v_{2,s}}{v_{2,r}} \right)^{1/3} - \frac{v_{2,s}}{2v_{2,r}} \right]}$$

where the \overline{M}_N is the number average molecular weight of PEGDA ($\overline{M}_N = 700$), V_1 is the molar volume of water ($V_1 = 18 \text{ mL mol}^{-1}$), \overline{v} is the specific volume of PEG ($\overline{v} = \frac{1}{\rho_P} = 0.893 \text{ cm}^3 \text{ g}^{-1}$), and χ_1 is the Flory PEG-water interaction parameter ($\chi_1 = 0.426$). The terms $v_{2,s}$ and $v_{2,r}$ are the volume fraction of polymers in the swelling states or relaxed states, respectively. Before measurements, the unbonded water was removed from the sample. All above constants are obtained from ref. ⁴⁶ An example was calculated in detail in Supporting Information.

3.4.6 Photorheology

In situ photorheology was carried out using an Anton Paar MCR 702 multidrive rheometer, as previously reported.⁴² Briefly, the sample was placed under the parallel plate (PP25) at a gap of 0.3 mm. The constant temperature (25 °C), normal force (0 N), shear strain (0.1%), and frequency (1 Hz) were applied. The LED placed under the lower glass plate was switched upon system stabilization. The dependent changes in the moduli of the investigated formulas during photopolymerization were measured as a function of exposure time.

3.4.7 Three-point bending tests

Three-point bending tests were carried out to measure the shape deformation of the polymeric materials. The measurements were conducted using Imada digital force gauge (ZTA-50N), with support pins placed 8.2 mm apart and a compression rate of 0.5 mm/min. The identical dimensions of the specimen were 20 mm × 3 mm × 2 mm (L × W × H).

3.4.8 3D printing

The digital light processing (DLP) 3D printer (MAKEX) equipped with a LED@405 nm (3 mW cm⁻²) was used for the 3D printing experiments. The layer thickness was 20 nm, and the layered exposure time was 10 seconds.

3.4.9 Electro-mechanical actuation

The electro-mechanical characterization of actuation was conducted as previously published.⁵¹ Briefly, the polymer strips were hanged and immersed in electric field. The electro stimulation

was applied by a power supply (PS-3005D). The tip displacements were recorded for the evaluation of actuation.

3.5 Results and discussion

3.5.1 Photophysical and photochemical characterization of naringin

Naringin demonstrated pH-mediated light absorption abilities, attributed to the hydroxyl groups on its chemical structure (Scheme 3.1). Confirmed by UV-vis spectra, the addition of NaOH induced red-shifted light absorption of naringin tailing to 525 nm (Figure 3.1), and the light absorption properties at the emission wavelength of the employed LED (400 nm) were improved. Specifically, in a neutral solution, naringin exhibited no absorption at 400 nm, but the light absorption was drastically increased to 16,200 M⁻¹ cm⁻¹ and 19,900 M⁻¹ cm⁻¹ in the presence of 100 mM and 500 mM NaOH, respectively (Table S3.1). Furthermore, compared to naringin in a neutral solution, the naringin solutions with the introduction of NaOH led to the appearance of new absorption peaks centered between 350 nm and 370 nm, assigned to the ionization and isomerization of chalcone-formed naringin. This trend aligned with the results reported previously.^{52, 53} Specifically, under basic conditions, the flavone-formed naringin was initially ionized forming corresponding primary and secondary conjugated bases with the increase of characterized light absorption at 280 nm (Scheme S3.1: step 1) in order at pHs < 12 (0.01 mM NaOH).⁵⁴ Subsequently, further alkali induced the formation of carbanions characterized by the presence of light absorption peak at 240 nm (Scheme S3.1: step 2).⁵³ Thereafter, with the continuous addition of NaOH, the ionized naringin and carbanion were increasingly produced, and the growing carbanion thus transformed slowly to chalcone formed naringin exhibited broad light absorption between 300 nm and 500 nm. (Scheme S3.1: step 3).⁵³ Chalcone-derived compounds have been widely explored as efficient photoinitiators under visible light.⁵⁵⁻⁵⁷ Therefore, the chalcone-formed naringin is a highly promising photoinitiator candidate.

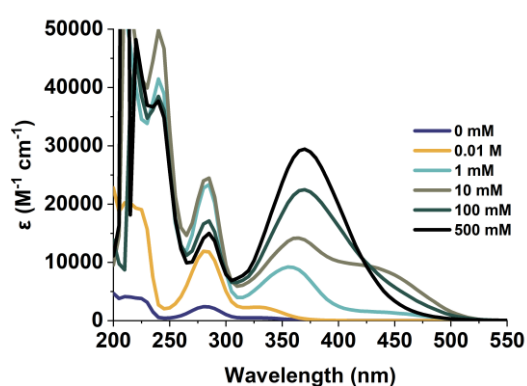


Figure 3.1. The UV-vis absorption of naringin in the aqueous media at diverse [NaOH].

To preliminarily assess the potential photoinitiation ability of naringin, steady-state photolysis in the presence of a coinitiator, iodonium salt (Iod), was carried out under the irradiation of LED@400 nm (Figure 3.2a). Upon the light irradiation, chalcone-formed naringin was excited, and an obvious decrease of light absorption at 370 nm was observed after a 10-second exposure. In addition, further photolysis occurred with additional irradiation time (Figure 3.2a). With the understanding of the photolysis that occurred between naringin and Iod, the formed active radical was characterized using the EPR-ST technique (Figure 3.2b). The free radical was identified as phenyl radical in line with the hyperfine splitting constants ($a_N = 14.3$ G, $a_H = 2.2$ G).⁵⁸ The generated phenyl radicals (Scheme 3.2) were the active species to initiate the following polymerization, followed by further propagation.

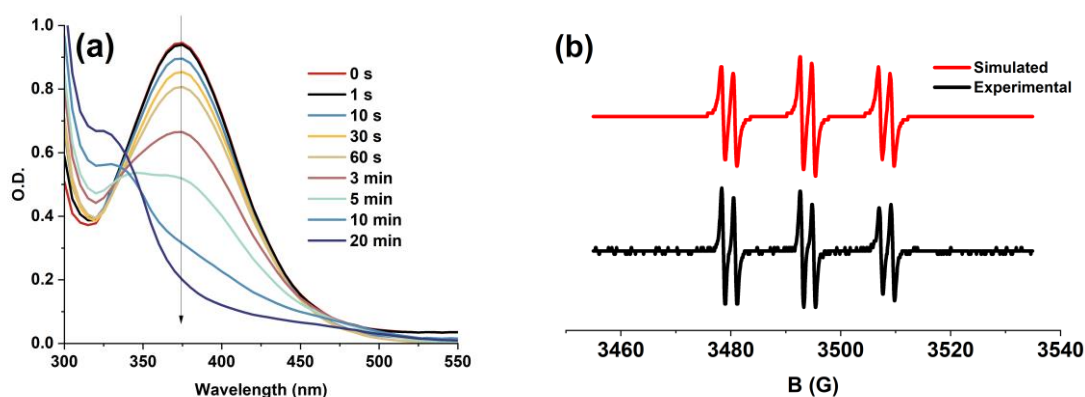
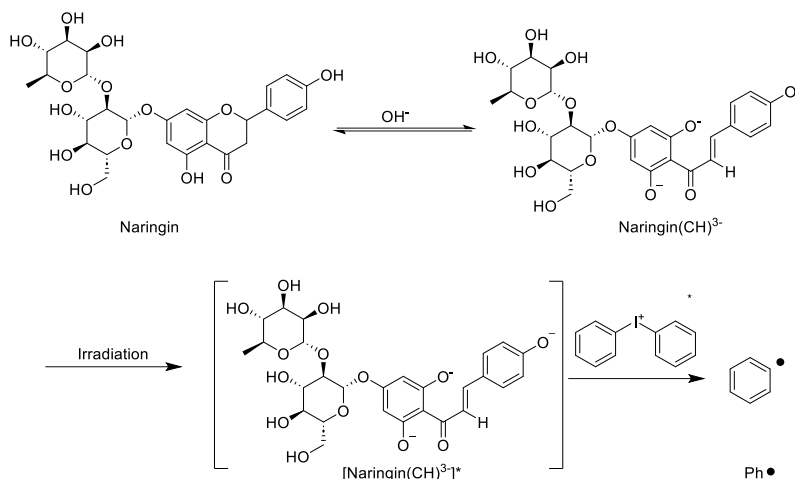


Figure 3.2. The interaction between naringin and Iod: (a) the steady-state photolysis of naringin/Iod in aq. NaOH upon exposure to LED@400 nm; UV-vis spectra were recorded at different irradiation time. ([NaOH] = 100 mM; [Iod] = 4.4 mM) and (b) EPR spectra of the radicals generated in naringin/Iod combination upon exposure to LED@400 nm and trapped by PBN in tert-butylbenzene: PBN/phenyl radical adducts formed in naringin/Iod system: $a_N = 14.3$ G, $a_H = 2.2$ G.⁵⁸



Scheme 3.2. The proposed photochemical mechanism on the generation of free radicals in naringin/Iod combination.^{52, 53, 59, 60}

*Naringin(CH): chalcone-formed naringin

3.5.2 Photoinitiation ability of naringin in alkane formulas

To evaluate the photoinitiation ability of naringin, a system of compositions was developed. Specifically, naringin and Iod were employed as photoinitiator and coinitiator, respectively, and PEGDA was introduced as a hydrophilic photocurable oligomer. Under the irradiation of LED@400 nm, the photopolymerization of PEGDA/DI water (8/2, w/w) blend was observed in the presence of naringin, Iod, and NaOH (Figure 3.3a). With the increasing concentrations of NaOH, the final double bond conversions of PEGDA were improved correspondingly, and consequently, the highest conversion was observed in the presence of 100 mM NaOH. As aforementioned, the presence of NaOH could induce ionization and isomerization, producing chalcone-formed naringin. 100 mM NaOH drastically accelerated the rate of polymerization compared to the formulas in the presence of 10 - 60 mM NaOH, in line with the excellent photoinitiation abilities of chalcone derivatives.⁵⁵⁻⁵⁷

Moreover, the NaOH-mediated photoinitiation ability of naringin indirectly affected mesh sizes and curing depths. Owing to its different crosslinking degrees, the inner mesh sizes of the network vary (Figure 3.3b). Specifically, the mesh sizes of crosslinking networks varied from 15 Å to 23 Å for the formula with 30 - 100 mM NaOH correspondingly (Figure 3.3b and Figure S3.1). Briefly, the higher final double bond conversion corresponded to the lower mesh size for the same photocurable resin mixture. As reported,^{50, 61} the mesh size determines the water uptake of hydrogels. In addition, the concentrations of NaOH also impacted the curing depth (Figure S3.1). As 100 mM NaOH accelerated and improved the polymerization of PEGDA photoinitiated by naringin, the rapid photopolymerization of PEGDA was observed, hence inducing further photopolymerization at the next sample layer. Therefore, at 100 mM NaOH,

with the most efficient photoinitiation ability, the deepest curing with 1.7-mm thickness was observed among the three investigated formulas (30 – 100 mM NaOH). In short, the concentration of NaOH could mediate mesh size of network and curing depth, which impacted the formula of 3D resin for actuator.

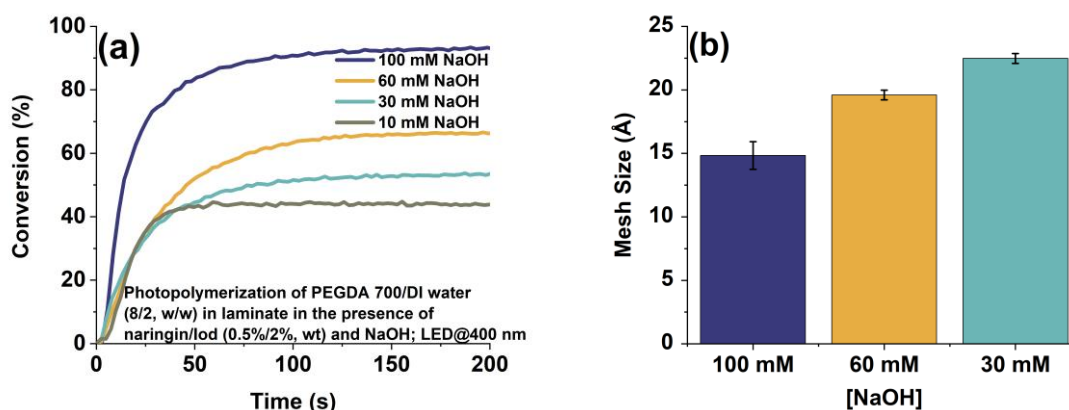


Figure 3.3. (a) Photopolymerization profiles (double bond conversions vs time) of PEGDA/DI water (8/2, w/w) in laminate in the presence of naringin/Iod (0.5%/2%, wt) with diverse [NaOH] upon the exposure to LED@400 nm (6.4 mW cm^{-2}) and (b) mesh sizes of the corresponding polymerized hydrogels.⁴⁶⁻⁵⁰

With the understanding of NaOH enhancement, further investigation on the effect of cation and anion was investigated. KOH and NaCl were employed in the photo-resin respectively with NaOH (Figure S3.2). In the event of identical hydroxide concentration, the photopolymerization profiles of PEGDA were comparable (Figure S3.2a). Typically, the final double bond conversions of PEGDA were > 95% in diverse ratios of NaOH/KOH, thus indicating cations exhibited little effect on the photoinitiation ability of naringin. Contrarily, the hydroxide concentration dominated the photoinitiation ability of naringin. Specifically, with the reduction of hydroxide concentration, the photopolymerization of PEGDA was drastically reduced. Only 42% acrylate conversion was observed for the formula with 10 mM NaOH (Figure S3.2b). Furthermore, with the addition of NaCl, the photopolymerization of the PEGDA profile almost overlapped with the one without NaCl in terms of both final double bond conversion and rate of polymerization (Figure S3.2b). The same photoinitiation behavior of naringin in NaOH (10 mM) and NaOH/NaCl (10 mM/90 mM) formulas suggested no effect of sodium and chloride ions on the photoinitiation ability of naringin. Therefore, OH^- is the only component able to improve the photoinitiation ability of naringin. Consequently, 100 mM NaOH was confirmed as a component in the resulting formula. Additionally, to confirm the effect of the coinitiator chemical structure, another onium salt, sulfonium (Scheme 3.1: SFO), was employed. In the identical conditions, the SFO extensively impeded the photopolymerization of PEGDA,

compared to the Iod-involved formula (Figure S3.3). Therefore, Iod was selected as a coinitiator for the following studies.

3.5.3 Development of naringin-based photoinitiating system for 3D printing of electro-active actuator

Considering the emission wavelength of the irradiation source in the digital light processing (DLP) 3D printer centered at 405 nm, the excellent photoinitiation ability of a naringin-based photoinitiating system under irradiation of LED@400 nm with low light intensity (6.4 mW cm^{-2}) as studied above can endow the developed prepolymer with high potential of 3D printability. However, the overloaded photoinitiator may inhibit photoinitiating system dissolution and light penetration, thus impeding photopolymerization, as previously reported.⁴² Therefore, the optimum concentration of naringin should be determined (Figure 3.4a). Upon exposure to LED@400 nm, the increasing amount of naringin improved the final acrylate conversion of PEGDA in the formula of PEGDA/DI water (8/2, w/w) in the presence of 100 mM NaOH. Typically, 0.1 wt% naringin (Figure 3.4a) reached over the critical concentration of naringin for photopolymerization of PEGDA under irradiation of LED@400 nm, and 33% of conversion was achieved (Table S3.2). With the accumulated concentration of naringin, the conversion of PEGDA reached 93% until 0.5 wt% naringin (Figure 3.4a and Table S3.2).

Additionally, for electro-active devices, a conductive component is essential, for example, charged/ionic components.^{19, 62-65} Specifically, the mobile ions migrate to the corresponding electrode (i.e., cathode/anode), and the polyions tend to their counterions direction. Due to the repulsion effect among the polyions, the equilibrium water content would be increased at the polyion aggregations side.⁶² In this regard, the negatively charged sodium acrylate (Scheme 3.1) was employed in the 3D resin formula. The introduction of sodium acrylate demanded additional water content in formulas for its sufficient dissolution, therefore, water content effect on the photopolymerization of PEGDA/DI water was investigated first. Compared to PEGDA/DI water (8/2, w/w), the PEGDA/DI water (6/4, wt) in the presence of the identical photoinitiating system afforded only 62% double bond conversion (Figure 3.4b and Table S3.3). Furthermore, the addition of water content also drastically affected the stability of the developed formulas. Specifically, the formulas of PEGDA/DI water (8/2, w/w) demonstrated fair stability after 5-min storage in ambient conditions, and the conversion differences were less than 5%, irrelative to naringin concentrations (Table S3.2). However, the additional 20 wt% water (PEGDA/DI water (6/4, w/w)) resulted in undesirable instability. Specifically, the conversion was reduced by 14% after 5 min (Table S3.3). Furthermore, the photoinitiation ability of naringin vanished in the water overloaded formula (PEGDA/DI water (4/6, w/w)) (Table S3.3). Before moving forward

on the determination of sodium acrylate amount, the 3D printability of water-borne formula has to be confirmed. With the abovementioned results, the PEGDA/DI water (8/2, w/w) in the presence of naringin/Iod (0.5%/2%, wt) was employed to the studies of 3D printability.

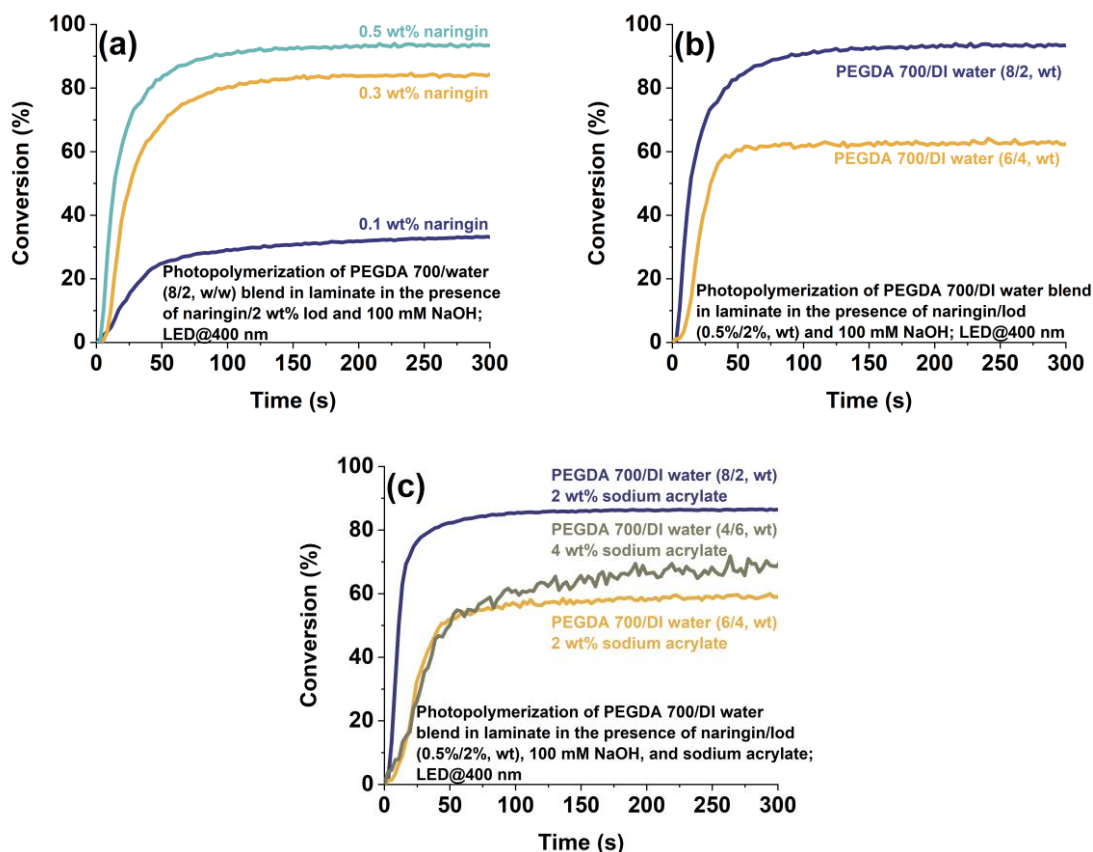


Figure 3.4. Photopolymerization profiles (double bond conversions vs time) of (a) PEGDA/DI water (8/2, w/w) blend in the presence of naringin/Iod (0.5%/2%, wt), (b) PEGDA/DI water in the presence of naringin/Iod (0.5%/2%, wt), and (c) PEGDA/DI water in the presence of naringin/Iod (0.5%/2%, wt) and sodium acrylate, with 100 mM NaOH in laminate upon exposure to the LED@400 nm (6.4 mW cm⁻²).

With the optimized prepolymer, a transparent yellow figurine of the Groot model was successfully 3D printed in ambient conditions (Figure 3.5). Specifically, the dimensions of this 3D printed figurine were 40 × 23 × 33 mm, L × W × H (Figure 3.5). Furthermore, the details of surface texture of 3D printed Groot were observed as well. Particularly, its eyes and smile on the 3D-printed figurine were obvious and evident. With the favorable 3D printability, the developed 3D resin could be involved in customized actuators with optimization.

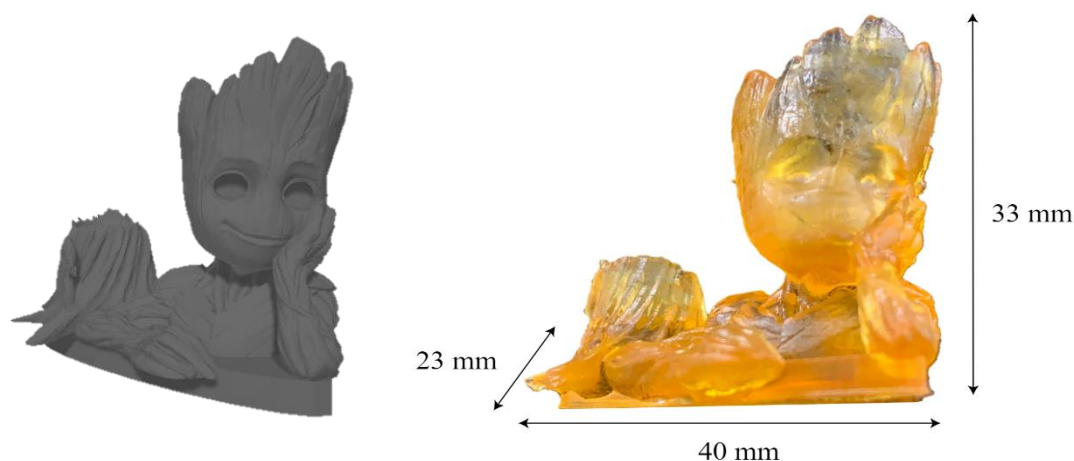


Figure 3.5. The front view of the STL model file and the Groot 3D printed using the PEGDA/DI water (8/2, w/w) in the presence of naringin/Iod (0.5%/2%, wt) and 100 mM NaOH. (40 × 23 × 33 mm, L × W × H; layered exposure time: 10 s)

Furthermore, as aforementioned, sodium acrylate is the conductive component for the designed formula of actuator 3D resins. In this regard, the real-time FTIR and in situ photorheology studies were carried out to evaluate the effect of the introduction of sodium acrylate on the photopolymerization of the developed 3D resin (Figure 3.4c). Typically, the addition of sodium acrylate rarely impacted the final conversion of PEGDA polymerization. The addition of 2 wt% sodium acrylate led to the difference of conversions by ~5% for the formulas of PEGDA/DI water (8/2, w/w) blend and PEGDA/DI water (6/4, w/w) blend (Table S3.3 and Table S3.4). Additionally, as expected, the additional 20 wt% water led to a vanished photoinitiation ability of the developed naringin-based photoinitiating system. However, the PEDGA/DI water (4/6, w/w) was successfully photocured with the addition of 4 wt% sodium acrylate (Table S3.4). Interestingly, the introduction of sodium acrylate improved the stability of the formulas, and the conversions reduced by only 9% after 5 min for PEDGA/DI water (6/4, w/w), compared to 14% conversion difference for the formula in the absence of sodium acrylate. To confirm the effectiveness of employed sodium acrylate, the electro-active actuation behavior was evaluated thereafter.

3.5.4 3D-printed actuator

With the developed 3D resin for electro-active actuators, the electro-sensitivities of the most stable formulas were evaluated by the displacement of the polymer strip tip (Scheme S3.2). In an applied electric field at the voltage of 30 V, the polymer strip without sodium acrylate exhibited a latent response (Figure 3.6a and S4a). The little displacement could be attributed to the electrocatalytic reaction driven fluid flow. Specifically, in the presence of electric field, the electrolysis of water occurred,⁶⁶ and ion flux resulted in concentration gradient, thus

forming fluid flow.⁶⁷ In the presence of sodium acrylate, obvious displacement was observed (Figure S3.4b1). Typically, with an electric field applied, the mobile cations and anions move to the cathode and anode, respectively. Therefore, the polyions (i.e., carboxyl anions) and mobile anions repel each other, thus forming a concentration gradient of the polyions in polymer networks. The equilibrium water content was therefore increased gradually in the direction from cathode to anode (Figure S3.4b1). Specifically, the anode side polymer exhibited swelling behavior, and the cathode side polymer exhibited shrink behavior.⁶² Furthermore, for the polymer in the presence of 4 wt% sodium acrylate, its displacement in the applied electric field reached its extent of 4 mm after only 3 min (Figure 3.6a). Interestingly, swapping the placement of the electrodes induced the strip movement towards the other direction (Figure 3.6b and Figure S3.4b2). Specifically, the movement of the polymeric strips was all towards the cathode regardless of the electrode position. Therefore, the electric field demonstrated its indispensable effect on the movement of the designed actuators.

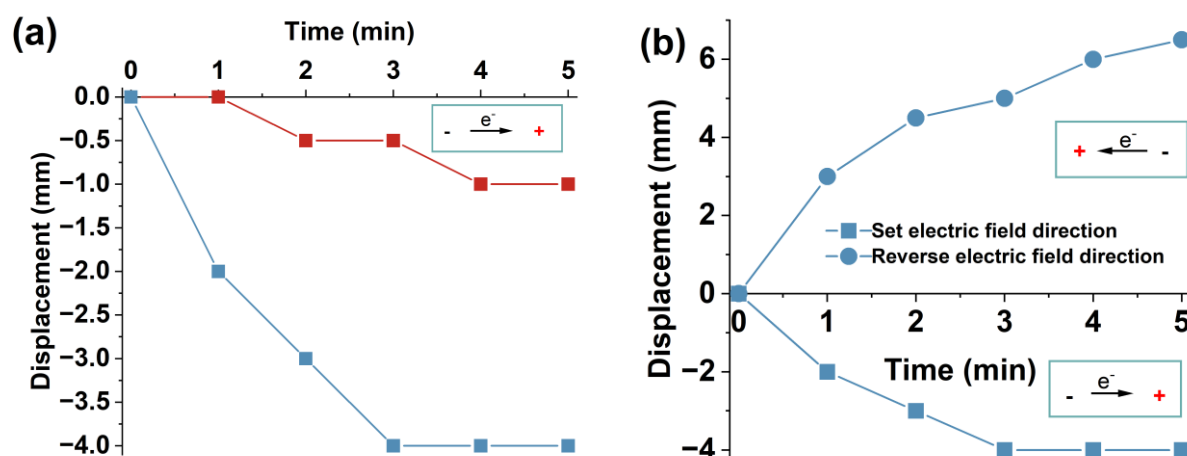


Figure 3.6. The actuation distance (distance vs time) of the electro-stimulated strips fabricated by (a) PEGDA/DI water (8/2, w/w) (red) and PEGDA/DI water (4/6, w/w) in the presence of 4 wt% sodium acrylate (blue), with 100 mM NaOH in an electric field (30 V) and (b) PEGDA/DI water (4/6, w/w) in the presence of 4 wt% sodium acrylate with 100 mM NaOH at set and reverse directions of the electric field.

Considering the electric field-induced polymer deformation (Figure S3.4), the mechanical strengths of the fabricated polymers were evaluated by three-point bending tests (Figure S3.5). With identical polymer dimensions, the increase of water content in the polymers in the absence of sodium acrylate dropped the mechanical strength from 1.6 N to 1.1 N. The same trend was observed in the polymers in the presence of sodium acrylate. In addition, with the introduction of sodium acrylate, the mechanical strengths were also reduced (Figure S3.5). These could be ascribed to the decreased double bond conversions (Figure 3.4b and c). As

the formula of PEGDA/DI water (4/6, w/w) in the presence of naringin/Iod (0.5%/2%. wt) and 100 mM NaOH can only be photocured with the addition of 4 wt% SA (Table S3.3 and Table S3.4), it was then involved in three-point bending test additionally. As predicted, the additional water content and SA synergistically resulted in a lowest mechanical strength of PEGDA/DI water (4/6, w/w) in the presence of 4 wt% sodium acrylate among all the samples (Figure S3.5). However, the formula in the presence of 4 wt% sodium acrylate exhibited higher double bond conversion (Figure 3.4c: 68%) compared with the one in the presence of 2 wt% sodium acrylate. Therefore, the reduction of mechanical strength of this formula could be mainly ascribed to the difference of water content caused diluted crosslinking densities. Typically, higher crosslinking density results in higher mechanical strength.⁶⁸ Comprehensively, the 2 wt% sodium acrylate in the formula of PEGDA/DI water (6/4, w/w) could be responsible for both the electro-sensitivity and flexibility of formed actuator.

With the determined naringin employed formula, two actuators were successfully 3D printed (Figure 3.7). Specifically, a hand-like model was successfully 3D printed (Figure 3.7a). At the beginning of the electric field applied, the hand-like object was planar (Figure 3.7a1). Thereafter, upon the electric field applied, the hand-like object was motivated to deform towards the cathode direction (Figure 3.7a2). With this concept, the design of actuators can therefore meet different requirements in diverse scenarios. For instance, a hook-like object was also successfully 3D printed using 0.3 mL (~0.3 g) resin in the same condition (Figure 3.7b). The planar hook was placed under water (Figure 3.7b1). Subsequently, upon electric field appearance, the planar object was transformed into a hook (Figure 3.7b2). Subsequently, the transformed hook successfully hooked the loads (Figure 3.7b3: 2.2 g). Furthermore, given that 6.6-g weight can be loaded on all three arms (Figure 3.7b4), indicating the strength to weight ratio was ~22. Consequently, its functionality for its underwater activities was successfully demonstrated. Therefore, with an appropriate design of a more dedicated structure and programmed electric field, the 3D printed actuator using the naringin employed formula can promisingly achieve complex geometry transformation and desired activities in water environment.

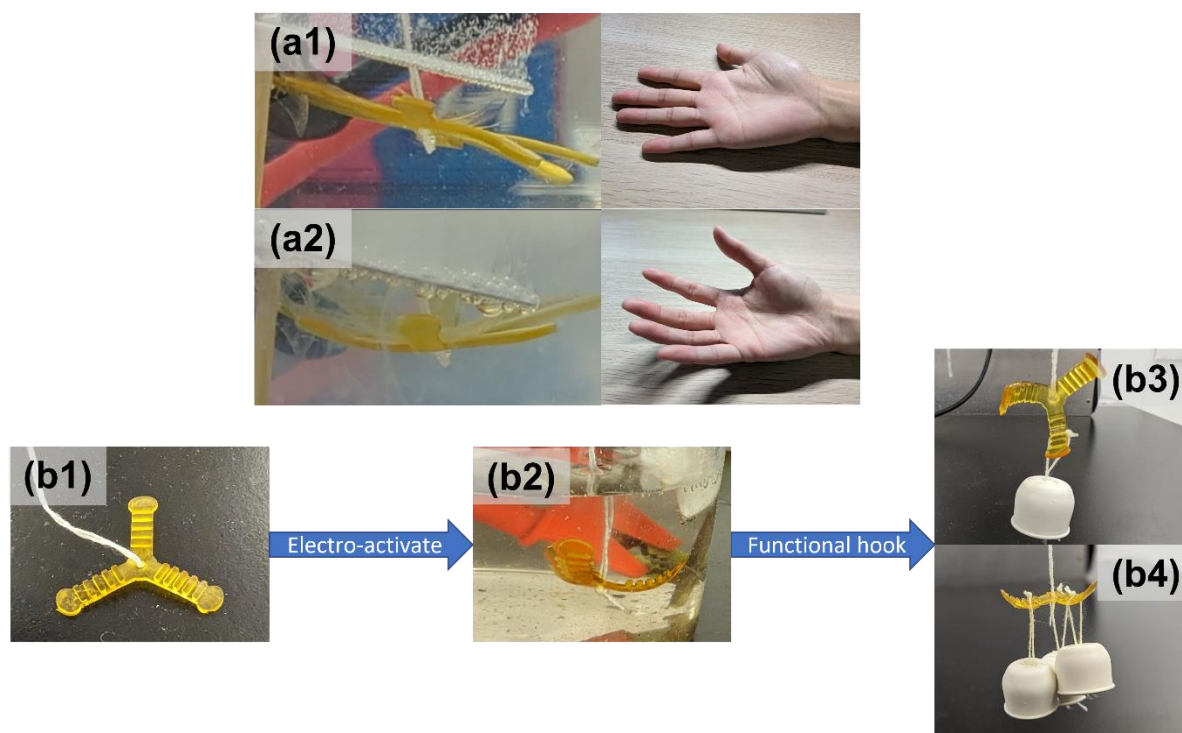


Figure 3.7. 3D printed electro-activated (a) hand-like actuators: (a1) before and (a2) after electro-stimulation; and (b) hook (PEGDA/DI water (6/4, w/w) in the presence of 2 wt% sodium acrylate with 100 mM NaOH): (b1) before, (b2) after electro-stimulation in an electric field (voltage = 30 V), and their loading of (b3) 2.2 g and (b4) 6.6 g.

3.6 Conclusion

In the present work, we have demonstrated the remarkable photoinitiation ability of naringin for DLP 3D printing. Specifically, our exploration revealed that the introduction of Na^+ rather than OH^- significantly enhanced naringin's photoinitiation ability, leading to rapid photopolymerization of PEGDA at a concentration of 100 mM NaOH. Utilizing this initial formula, a high-fidelity Groot figurine with detailed surface texture was successfully 3D printed. In addition, by incorporating sodium acrylate, we observed electro-active actuation behavior under an applied electric field. However, it became evident that while sodium acrylate contributed to electro-sensitivity, it also compromised the mechanical strength of the material. Consequently, after meticulous experimentation, we determined an optimal concentration of sodium acrylate (2 wt%) for the 3D resin used in actuator production. Employing this optimized formula, a hand-like and a hook-like hydrogel devices were fabricated using the 3D printing technique. The hand-like hydrogel device exhibited actuation behavior akin to human grasping movements, while the hook-like hydrogel device showcased its ability to transform from a planar status under an electric field, affirming its loads-bearing ability. Given its excellent 3D printability, the developed 3D resin exhibited the capability to fabricate intricate structures. By combining tailored designs and programmed electric field, 3D printed actuators using the

naringin-based resin hold promise for fulfilling proposed functions in aqueous environments like tissue fluid. This breakthrough significantly broadens its potential applications in bioengineering.

3.7 References:

- (1) Dickens, S. H.; Stansbury, J. W.; Choi, K. M.; Floyd, C. J. E. Photopolymerization Kinetics of Methacrylate Dental Resins. *Macromolecules* **2003**, *36* (16), 6043-6053.
- (2) Apsite, I.; Salehi, S.; Ionov, L. Materials for Smart Soft Actuator Systems. *Chem. Rev.* **2022**, *122* (1), 1349-1415.
- (3) Fonseca, A. C.; Melchels, F. P. W.; Ferreira, M. J. S.; Moxon, S. R.; Potjewyd, G.; Dargaville, T. R.; Kimber, S. J.; Domingos, M. Emulating Human Tissues and Organs: A Bioprinting Perspective Toward Personalized Medicine. *Chem. Rev.* **2020**, *120* (19), 11128-11174.
- (4) Bonardd, S.; Nandi, M.; Hernandez Garcia, J. I.; Maiti, B.; Abramov, A.; Diaz Diaz, D. Self-Healing Polymeric Soft Actuators. *Chem. Rev.* **2023**, *123* (2), 736-810.
- (5) Sun, W. J.; Guan, Y.; Wang, Y. Y.; Wang, T.; Xu, Y. T.; Kong, W. W.; Jia, L. C.; Yan, D. X.; Li, Z. M. Low-Voltage Actuator with Bilayer Structure for Various Biomimetic Locomotions. *ACS Appl. Mater. Interfaces* **2021**, *13* (36), 43449-43457.
- (6) Yang, R.; Zhao, Y. Non-Uniform Optical Inscription of Actuation Domains in a Liquid Crystal Polymer of Uniaxial Orientation: An Approach to Complex and Programmable Shape Changes. *Angew. Chem., Int. Ed.* **2017**, *56* (45), 14202-14206.
- (7) Yang, C.; Shi, X.; Deng, H.; Du, Y. Antifatigue Hydration-Induced Polysaccharide Hydrogel Actuators Inspired by Crab Joint Wrinkles. *ACS Appl. Mater. Interfaces* **2022**, *14* (4), 6251-6260.
- (8) Xue, J.; Ge, Y.; Liu, Z.; Liu, Z.; Jiang, J.; Li, G. Photoprogrammable Moisture-Responsive Actuation of a Shape Memory Polymer Film. *ACS Appl. Mater. Interfaces* **2022**, *14* (8), 10836-10843.
- (9) Wang, W.; Xu, X.; Zhang, C.; Huang, H.; Zhu, L.; Yue, K.; Zhu, M.; Yang, S. Skeletal Muscle Fibers Inspired Polymeric Actuator by Assembly of Triblock Polymers. *Adv. Sci.* **2022**, *9* (13), e2105764.
- (10) Ge, Y.; Wang, H.; Xue, J.; Jiang, J.; Liu, Z.; Liu, Z.; Li, G.; Zhao, Y. Programmable Humidity-Responsive Actuation of Polymer Films Enabled by Combining Shape Memory Property and Surface-Tunable Hygroscopicity. *ACS Appl. Mater. Interfaces* **2021**, *13* (32), 38773-38782.
- (11) Wei, S.; Lu, W.; Le, X.; Ma, C.; Lin, H.; Wu, B.; Zhang, J.; Theato, P.; Chen, T. Bioinspired Synergistic Fluorescence-Color-Switchable Polymeric Hydrogel Actuators. *Angew. Chem., Int. Ed.* **2019**, *58* (45), 16243-16251.
- (12) Farhan, M.; Rudolph, T.; Nochel, U.; Yan, W.; Kratz, K.; Lendlein, A. Noncontinuously Responding Polymeric Actuators. *ACS Appl. Mater. Interfaces* **2017**, *9* (39), 33559-33564.
- (13) Nakahata, M.; Takashima, Y.; Hashidzume, A.; Harada, A. Redox-generated mechanical motion of a supramolecular polymeric actuator based on host-guest interactions. *Angew. Chem., Int. Ed.* **2013**, *52* (22), 5731-5735.
- (14) Yu, H.; Ikeda, T. Photocontrollable liquid-crystalline actuators. *Adv. Mater.* **2011**, *23* (19), 2149-2180.
- (15) Ilami, M.; Bagheri, H.; Ahmed, R.; Skowronek, E. O.; Marvi, H. Materials, Actuators, and Sensors for Soft Bioinspired Robots. *Adv. Mater.* **2021**, *33* (19), e2003139.
- (16) Mirvakili, S. M.; Hunter, I. W. Artificial Muscles: Mechanisms, Applications, and Challenges. *Adv. Mater.* **2018**, *30* (6), 1704407.

- (17) Zeng, H.; Wasylczyk, P.; Wiersma, D. S.; Priimagi, A. Light Robots: Bridging the Gap between Microrobotics and Photomechanics in Soft Materials. *Adv. Mater.* **2018**, *30* (24), e1703554.
- (18) Baumgartner, R.; Kogler, A.; Stadlbauer, J. M.; Foo, C. C.; Kaltseis, R.; Baumgartner, M.; Mao, G.; Keplinger, C.; Koh, S. J. A.; Arnold, N.; et al. A Lesson from Plants: High-Speed Soft Robotic Actuators. *Adv. Sci.* **2020**, *7* (5), 1903391.
- (19) Han, D.; Farino, C.; Yang, C.; Scott, T.; Browe, D.; Choi, W.; Freeman, J. W.; Lee, H. Soft Robotic Manipulation and Locomotion with a 3D Printed Electroactive Hydrogel. *ACS Appl. Mater. Interfaces* **2018**, *10* (21), 17512-17518.
- (20) López - Díaz, A.; Martín - Pacheco, A.; Rodríguez, A. M.; Herrero, M. A.; Vázquez, A. S.; Vázquez, E. Concentration Gradient - Based Soft Robotics: Hydrogels Out of Water. *Adv. Funct. Mater.* **2020**, *30* (46), 2004417.
- (21) Gladman, A. S.; Matsumoto, E. A.; Nuzzo, R. G.; Mahadevan, L.; Lewis, J. A. Biomimetic 4D printing. *Nat. Mater.* **2016**, *15* (4), 413-418.
- (22) van Oosten, C. L.; Bastiaansen, C. W.; Broer, D. J. Printed artificial cilia from liquid-crystal network actuators modularly driven by light. *Nat. Mater.* **2009**, *8* (8), 677-682.
- (23) Li, T.; Li, G.; Liang, Y.; Cheng, T.; Dai, J.; Yang, X.; Liu, B.; Zeng, Z.; Huang, Z.; Luo, Y.; et al. Fast-moving soft electronic fish. *Sci. Adv.* **2017**, *3* (4), e1602045.
- (24) Ligon, S. C.; Liska, R.; Stampfl, J.; Gurr, M.; Mulhaupt, R. Polymers for 3D Printing and Customized Additive Manufacturing. *Chem. Rev.* **2017**, *117* (15), 10212-10290.
- (25) Zhu, D.; Zhang, J.; Lalevée, J.; Xiao, P. Chapter 1 Novel Photoinitiating Systems for 3D Printing. In *3D Printing with Light*, Xiao, P., Zhang, J. Eds.; De Gruyter, 2021; pp 1-48.
- (26) Lee, M.; Rizzo, R.; Surman, F.; Zenobi-Wong, M. Guiding Lights: Tissue Bioprinting Using Photoactivated Materials. *Chem. Rev.* **2020**, *120* (19), 10950-11027.
- (27) Popal, M.; Volk, J.; Leyhausen, G.; Geurtsen, W. Cytotoxic and genotoxic potential of the type I photoinitiators BAPO and TPO on human oral keratinocytes and V79 fibroblasts. *Dent. Mater.* **2018**, *34* (12), 1783-1796.
- (28) Chartrain, N. A.; Williams, C. B.; Whittington, A. R. A review on fabricating tissue scaffolds using vat photopolymerization. *Acta Biomater.* **2018**, *74*, 90-111.
- (29) You, S.; Xiang, Y.; Hwang, H. H.; Berry, D. B.; Kiratitanaporn, W.; Guan, J.; Yao, E.; Tang, M.; Zhong, Z.; Ma, X.; et al. High cell density and high-resolution 3D bioprinting for fabricating vascularized tissues. *Science Advances* **2023**, *9* (8), eade7923.
- (30) Noirbent, G.; Dumur, F. Photoinitiators of polymerization with reduced environmental impact: Nature as an unlimited and renewable source of dyes. *Eur. Polym. J.* **2021**, *142*, 110109.
- (31) Zhu, D.; Peng, X.; Xiao, P. Penta - Hydroxy Flavones - Based Photoinitiating Systems for Free Radical, Cationic, and Thiol - Ene Polymerization upon Exposure to Mild Blue LEDs. *Macromol. Mater. Eng.* **2021**, *306* (6), 2100059.
- (32) Wu, C.; Shanmugam, S.; Xu, J.; Zhu, J.; Boyer, C. Chlorophyll a crude extract: efficient photo-degradable photocatalyst for PET-RAFT polymerization. *Chem. Commun.* **2017**, *53* (93), 12560-12563.
- (33) Shanmugam, S.; Xu, J.; Boyer, C. Utilizing the electron transfer mechanism of chlorophyll a under light for controlled radical polymerization. *Chem. Sci.* **2015**, *6* (2), 1341-1349.
- (34) Zhao, J.; Lalevée, J.; Lu, H.; MacQueen, R.; Kable, S. H.; Schmidt, T. W.; Stenzel, M. H.; Xiao, P. A new role of curcumin: as a multicolor photoinitiator for polymer fabrication under household UV to red LED bulbs. *Polym. Chem.* **2015**, *6* (28), 5053-5061.
- (35) Breloy, L.; Ouarabi, C. A.; Brosseau, A.; Dubot, P.; Brezova, V.; Abbad Andaloussi, S.; Malval, J.-P.; Versace, D.-L. β -Carotene/Limonene Derivatives/Eugenol: Green Synthesis of Antibacterial Coatings under Visible-Light Exposure. *ACS Sustainable Chem. Eng.* **2019**, *7* (24), 19591-19604.
- (36) Wollensak, G.; Spoerl, E.; Seiler, T. Riboflavin/ultraviolet-a-induced collagen crosslinking for the treatment of keratoconus. *Am. J. Ophthalmol.* **2003**, *135* (5), 620-627.

- (37) Chang, H. K.; Yang, D. H.; Ha, M. Y.; Kim, H. J.; Kim, C. H.; Kim, S. H.; Choi, J. W.; Chun, H. J. 3D printing of cell-laden visible light curable glycol chitosan bioink for bone tissue engineering. *Carbohydr. Polym.* **2022**, *287*, 119328.
- (38) Shin, D.; Hyun, J. Silk fibroin microneedles fabricated by digital light processing 3D printing. *J. Ind. Eng. Chem.* **2021**, *95*, 126-133.
- (39) Alam, M. A.; Subhan, N.; Rahman, M. M.; Uddin, S. J.; Reza, H. M.; Sarker, S. D. Effect of citrus flavonoids, naringin and naringenin, on metabolic syndrome and their mechanisms of action. *Adv. Nutr.* **2014**, *5* (4), 404-417.
- (40) Lavrador, P.; Gaspar, V. M.; Mano, J. F. Bioinspired bone therapies using naringin: applications and advances. *Drug Discovery Today* **2018**, *23* (6), 1293-1304.
- (41) Wong, R. W.; Rabie, A. B. Effect of naringin collagen graft on bone formation. *Biomaterials* **2006**, *27* (9), 1824-1831.
- (42) Zhu, D.; Peng, X.; Xiao, P. Indigo Carmine: A Base and Neutral Electrolyte-mediated Photoinitiator for 3D Printing in High Fidelity. *Addit. Manuf.* **2022**, *59*, 103154.
- (43) Witte, R. P.; Blake, A. J.; Palmer, C.; Kao, W. J. Analysis of poly(ethylene glycol)-diacrylate macromer polymerization within a multicomponent semi-interpenetrating polymer network system. *J. Biomed. Mater. Res., Part A* **2004**, *71* (3), 508-518.
- (44) Silverstein, R. M.; Webster, F. X.; Kiemle, D. J.; Bryce, D. L. *Spectrometric Identification of Organic Compounds*; Wiley, 2014.
- (45) Coates, J. Interpretation of Infrared Spectra, A Practical Approach. In *Encyclopedia of Analytical Chemistry*, 2006.
- (46) Richbourg, N. R.; Wancura, M.; Gilchrist, A. E.; Toubbeh, S.; Harley, B. A. C.; Cosgriff-Hernandez, E.; Peppas, N. A. Precise control of synthetic hydrogel network structure via linear, independent synthesis-swelling relationships. *Sci. Adv.* **2021**, *7* (7).
- (47) Slaughter, B. V.; Khurshid, S. S.; Fisher, O. Z.; Khademhosseini, A.; Peppas, N. A. Hydrogels in Regenerative Medicine. *Adv. Mater.* **2009**, *21* (32-33), 3307-3329.
- (48) Orwoll, R. A.; Arnold, P. A. *Physical properties of polymers handbook*; Springer, 2007.
- (49) Flory, P. J. *Principles of Polymer Chemistry*; Cornell University Press, 1953.
- (50) Canal, T.; Peppas, N. A. Correlation between mesh size and equilibrium degree of swelling of polymeric networks. *J. Biomed. Mater. Res.* **1989**, *23* (10), 1183-1193.
- (51) Yan, Y.; Santaniello, T.; Bettini, L. G.; Minnai, C.; Bellacicca, A.; Porotti, R.; Denti, I.; Faraone, G.; Merlini, M.; Lenardi, C.; et al. Electroactive Ionic Soft Actuators with Monolithically Integrated Gold Nanocomposite Electrodes. *Adv. Mater.* **2017**, *29* (23), 1606109.
- (52) González, E. A.; Nazareno, M. A.; Borsarelli, C. D. Enthalpy–entropy compensation effect in the chalcone formation from naringin in water–ethanol mixtures. *J. Chem. Soc., Perkin Trans. 2* **2002**, (12), 2052-2056.
- (53) Montenegro, M. A.; Nazareno, M. A.; Borsarelli, C. D. Kinetic study of the photosensitized oxygenation of the flavanone naringin and its chalcone. *J. Photochem. Photobiol., A* **2007**, *186* (1), 47-56.
- (54) Mielczarek, C. Acid-base properties of selected flavonoid glycosides. *Eur. J. Pharm. Sci.* **2005**, *25* (2-3), 273-279.
- (55) Chen, H.; Noirbent, G.; Liu, S.; Brunel, D.; Graff, B.; Gignes, D.; Zhang, Y.; Sun, K.; Morlet-Savary, F.; Xiao, P.; et al. Bis-chalcone derivatives derived from natural products as near-UV/visible light sensitive photoinitiators for 3D/4D printing. *Mater. Chem. Front.* **2021**, *5* (2), 901-916.
- (56) Chen, H.; Noirbent, G.; Sun, K.; Brunel, D.; Gignes, D.; Morlet-Savary, F.; Zhang, Y.; Liu, S.; Xiao, P.; Dumur, F.; et al. Photoinitiators derived from natural product scaffolds: monochalcones in three-component photoinitiating systems and their applications in 3D printing. *Polym. Chem.* **2020**, *11* (28), 4647-4659.
- (57) Chen, H.; Noirbent, G.; Zhang, Y.; Brunel, D.; Gignes, D.; Morlet-Savary, F.; Graff, B.; Xiao, P.; Dumur, F.; Lalevée, J. Novel D– π -A and A– π -D– π -A three-component photoinitiating systems based on carbazole/triphenylamino based chalcones and application in 3D and 4D printing. *Polym. Chem.* **2020**, *11* (40), 6512-6528.

- (58) Buettner, G. R. Spin trapping: ESR parameters of spin adducts. *Free Radical Biol. Med.* **1987**, 3 (4), 259-303.
- (59) Di Meo, F.; Lemaur, V.; Cornil, J.; Lazzaroni, R.; Duroux, J. L.; Olivier, Y.; Trouillas, P. Free radical scavenging by natural polyphenols: atom versus electron transfer. *J. Phys. Chem. A* **2013**, 117 (10), 2082-2092.
- (60) Kron, I.; Pudychová-Chovanová, Z.; Veliká, B.; Guzy, J.; Perjési, P. (E)-2-Benzylidenebenzocyclanones, part VIII: spectrophotometric determination of pK_a values of some natural and synthetic chalcones and their cyclic analogues. *Monatsh. Chem.* **2011**, 143 (1), 13-17.
- (61) Betz, M.; Hörmansperger, J.; Fuchs, T.; Kulozik, U. Swelling behaviour, charge and mesh size of thermal protein hydrogels as influenced by pH during gelation. *Soft Matter* **2012**, 8 (8), 2477-2485, 10.1039/C2SM06976H.
- (62) Shin, Y.; Choi, M. Y.; Choi, J.; Na, J. H.; Kim, S. Y. Design of an Electro-Stimulated Hydrogel Actuator System with Fast Flexible Folding Deformation under a Low Electric Field. *ACS Appl. Mater. Interfaces* **2021**, 13 (13), 15633-15646.
- (63) Li, Y.; Sun, Y.; Xiao, Y.; Gao, G.; Liu, S.; Zhang, J.; Fu, J. Electric Field Actuation of Tough Electroactive Hydrogels Cross-Linked by Functional Triblock Copolymer Micelles. *ACS Appl. Mater. Interfaces* **2016**, 8 (39), 26326-26331.
- (64) Cheedarala, R. K.; Jeon, J.-H.; Kee, C.-D.; Oh, I.-K. Bio-Inspired All-Organic Soft Actuator Based on a π - π Stacked 3D Ionic Network Membrane and Ultra-Fast Solution Processing. *Adv. Funct. Mater.* **2014**, 24 (38), 6005-6015.
- (65) Kim, O.; Shin, T. J.; Park, M. J. Fast low-voltage electroactive actuators using nanostructured polymer electrolytes. *Nat. Commun.* **2013**, 4, 2208.
- (66) Naito, T.; Shinagawa, T.; Nishimoto, T.; Takanabe, K. Water Electrolysis in Saturated Phosphate Buffer at Neutral pH. *ChemSusChem* **2020**, 13 (22), 5921-5933.
- (67) Ashaju, A. A.; Otten, V.; Wood, J. A.; Lammertink, R. G. H. Electrocatalytic Reaction Driven Flow: Role of pH in Flow Reversal. *J. Phys. Chem. C* **2021**, 125 (45), 24876-24886.
- (68) Du, Y.; Zhao, G.; Shi, G.; Wang, Y.; Li, W.; Ren, S. Effect of crosslink structure on mechanical properties, thermal stability and flame retardancy of natural flavonoid based epoxy resins. *Eur. Polym. J.* **2022**, 162, 110898.

3.8 Supporting Information

Mesh size calculation example

Formula of naringin: 0.5 wt%; Iod: 2 wt%; [NaOH] = 100 mM; PEGDA/water = 8/2, w/w

Number average molecular weight (\overline{M}_N) of PEGDA:

$$\overline{M}_N = 700 \text{ g mol}^{-1}$$

Weight of relaxed ($M_{relaxed}$), swollen ($M_{swollen}$), and dry (M_{dry}) example polymer:

$$M_{relaxed} = 0.1866 \text{ g}$$

$$M_{swollen} = 0.2809 \text{ g}$$

$$M_{dry} = 0.0694 \text{ g}$$

Polymer mass percentage of relaxed ($m_{relaxed}$) and swollen ($m_{swollen}$) example polymer:

$$m_{relaxed} = \frac{M_{dry}}{M_{relaxed}} = 0.372$$

$$m_{swollen} = \frac{M_{dry}}{M_{swollen}} = 0.247$$

Density of PEGDA 700 (ρ_P) and water (ρ_w):

$$\rho_P = 1.12 \text{ g mL}^{-1}$$

$$\rho_w = 1 \text{ g mL}^{-1}$$

Volume fraction of polymer in relaxed ($v_{2,r}$) and swollen states ($v_{2,s}$):

$$v_{2,r} = \frac{m_{relaxed}/\rho_P}{\frac{m_{relaxed}}{\rho_P} + \frac{(1 - m_{relaxed})}{\rho_w}} = 0.346$$

$$v_{2,s} = \frac{m_{swollen}/\rho_P}{\frac{m_{swollen}}{\rho_P} + \frac{(1 - m_{swollen})}{\rho_w}} = 0.226$$

Specific volume of polymer:

$$\bar{v} = \frac{1}{\rho_P} = 0.893 \text{ cm}^3 \text{ g}^{-1}$$

Flory polymer-solvent interaction parameter for PEG-water: $\chi_1 = 0.426$

Molar volume of water:

$$V_1 = 18 \text{ mL mol}^{-1}$$

All abovementioned values were substituted into the following equation:

$$\frac{1}{\bar{M}_C} = \frac{2}{\bar{M}_N} - \frac{(\bar{v}/V_1)[\ln(1 - v_{2,s}) + v_{2,s} + \chi_1 v_{2,s}^2]}{v_{2,r} \left[\left(\frac{v_{2,s}}{v_{2,r}} \right)^{1/3} - \frac{v_{2,s}}{2v_{2,r}} \right]}$$

then,

$$\bar{M}_C = 196.47 \text{ g mol}^{-1}$$

Bond length of the polymer backbone:

$$l = 1.54 \text{ \AA}$$

Characteristic ratio for PEG:

$$C_N = 4$$

Molecular weight of the repeat units:

$$M_r = 44.05 \text{ g mol}^{-1}$$

\bar{M}_C , l , C_N , and was then substituted into the following Flory-Rehner equation:

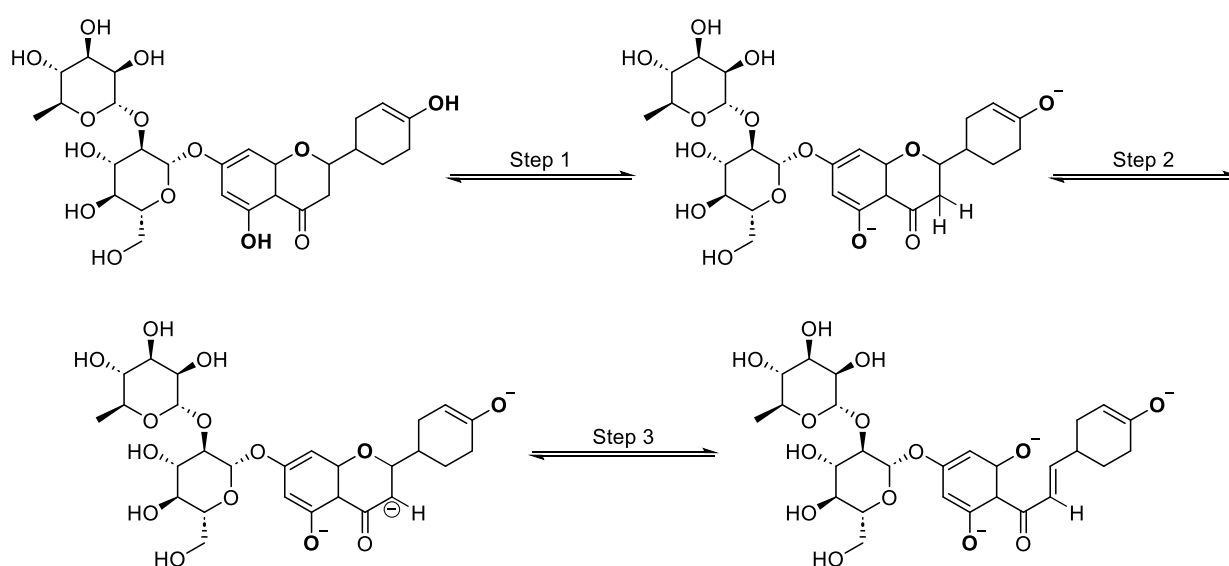
$$\xi = v_{2,s}^{-1/3} \left(\frac{2C_N \bar{M}_C}{M_r} \right)^{1/2} l$$

Consequently, the mesh size:

$$\xi = 15 \text{ \AA}$$

Table S3.1. Light absorption properties of naringin in diverse $[\text{NaOH}]_{\text{aq}}$: maximum absorption wavelengths λ_{max} , extinction coefficients at λ_{max} and at the maximum emission wavelengths of the investigated LED@400 nm.

$[\text{NaOH}]_{\text{aq}}$ (mM)	λ_{max} (nm)	ϵ_{max} ($\text{M}^{-1} \text{cm}^{-1}$)	$\epsilon_{400 \text{ nm}}$ ($\text{M}^{-1} \text{cm}^{-1}$)
0	280	2400	0
0.01	280	11,900	0
1	285	23,400	2500
	355	9200	
10	285	24,500	10,200
	365	14,200	
100	285	17,100	16,200
	370	22,500	
500	285	15,000	19,900
	370	29,400	



Scheme S3.1. The mechanism of ionization and isomerization of naringin.⁵³

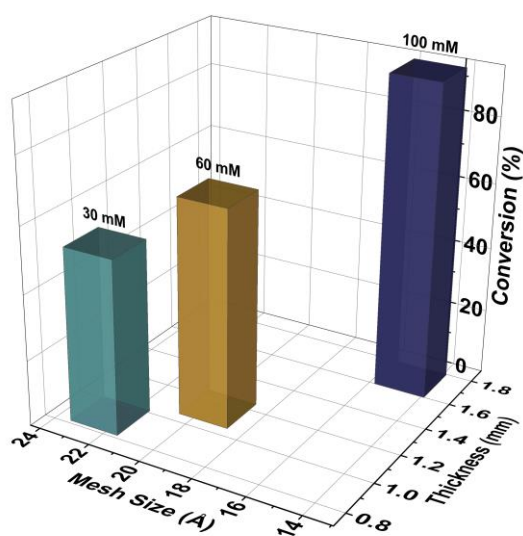


Figure S3.1. The relationships between mesh sizes, curing thicknesses, and C=C conversions of polymerized PEDGA 700/DI water (8/2, w/w) in the presence of naringin/Iod (0.5%/2%, wt) with diverse [NaOH] upon exposure of LED@400 nm (6.4 mW cm^{-2}).

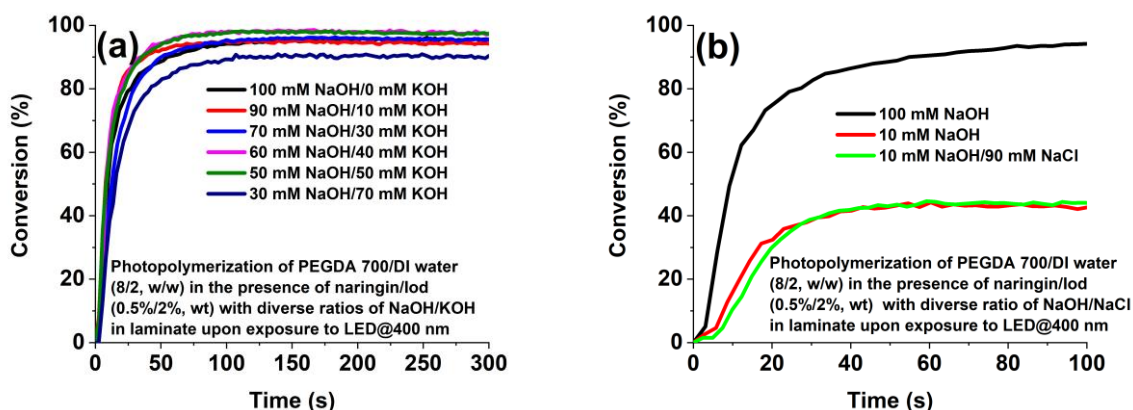


Figure S3.2. Photopolymerization profiles (double bond conversions vs time) of PEGDA 700/DI water (8/2, w/w) blends in the presence of naringin/Iod (0.5%/2%, wt) in laminate with diverse ratio of (a) NaOH/KOH and (b) NaOH/NaCl upon exposure to LED@400 nm (6.4 mW cm^{-2}).

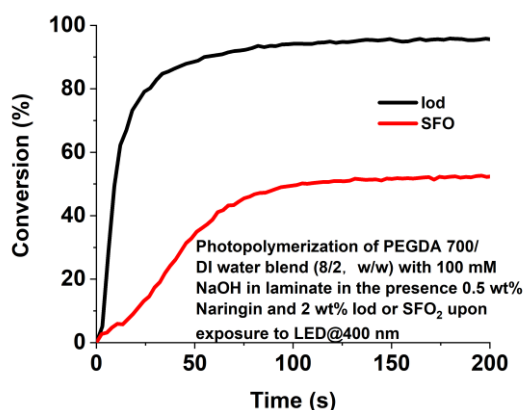


Figure S3.3. Photopolymerization profiles (double bond conversions vs time) of PEGDA 700/DI water (8/2, w/w) blends in the presence of naringin/Iod (0.5%/2%, wt) or naringin/SFO (0.5%/2%, wt) with 100 mM NaOH in laminate upon exposure to LED@400 nm (6.4 mW cm^{-2}).

Table S3.2. The stability of developed formulations in the presence of diverse naringin concentrations. (Iod: 2 wt%; PEGDA/DI water: 8/2, w/w; [NaOH] = 100 mM)

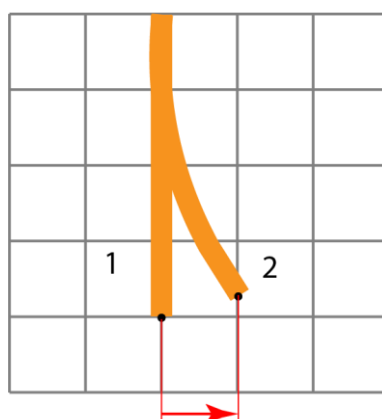
	Double bond conversions (%)	
	0 min	5 min
0.1 wt% naringin	33	29
0.3 wt% naringin	84	79
0.5 wt% naringin	93	90

Table S3.3. The stability of developed formulations in the presence of diverse PEGDA 700/DI water ratios. (Naringin: 0.5 wt%; Iod: 2 wt%; [NaOH] = 100 mM)

	Double bond conversions (%)	
	0 min	5 min
PEGDA 700/DI water (8/2, w/w)	93	90
PEGDA 700/DI water (6/4, w/w)	62	48
PEGDA 700/DI water (4/6, w/w)	0	0

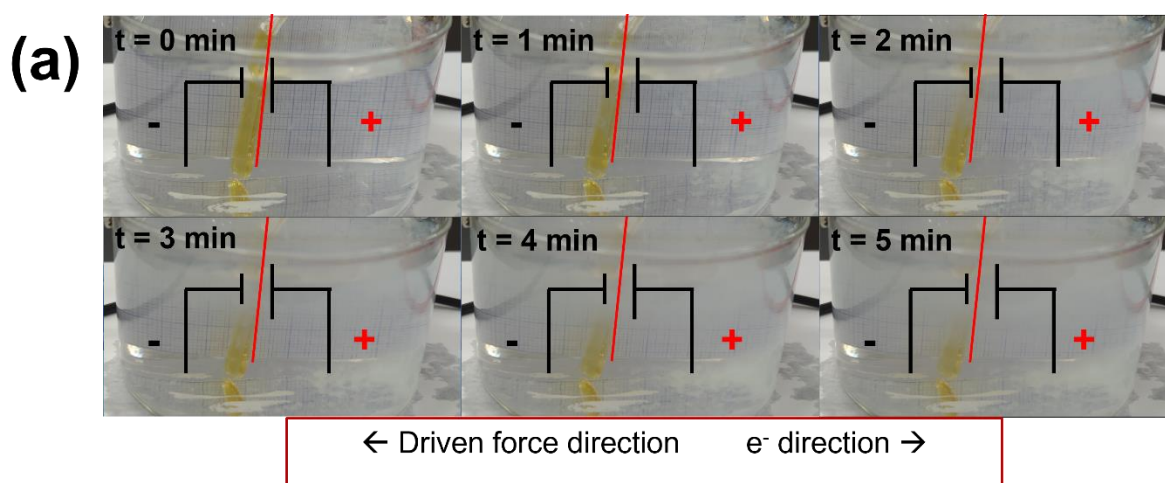
Table S3.4. The stability of developed formulations in the presence of diverse sodium acrylate concentrations. (Naringin: 0.5 wt%; Iod: 2 wt%; [NaOH] = 100 mM)

	Double bond conversions (%)	
	0 min	5 min
2 wt% sodium acrylate in PEGDA 700/DI water (8/2, w/w)	88	87
2 wt% sodium acrylate in PEGDA 700/DI water (6/4, w/w)	58	49
2 wt% sodium acrylate in PEGDA 700/DI water (4/6, w/w)	0	0
4 wt% sodium acrylate in PEGDA 700/DI water (4/6, w/w)	68	68



Displacement

Scheme S3.2. The displacement measurement of the photopolymerized strip under the electro-stimulated actuation.



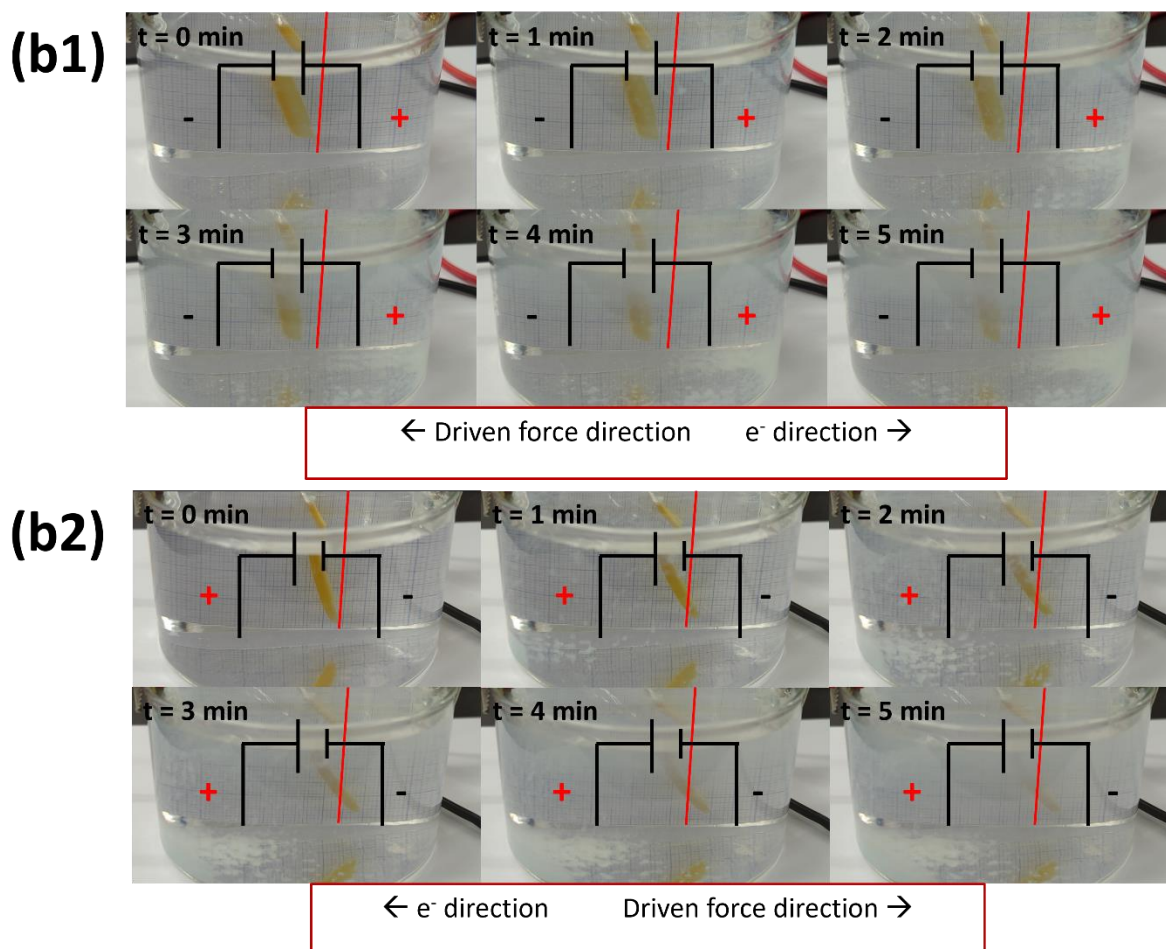


Figure S3.4. Electro-stimulated actuation of the strips ($40 \times 10 \times 2$ mm) fabricated by (a) PEGDA 700/DI water (8/2, w/w) and (b) PEGDA 700/DI water (4/6, w/w) in the presence of 4 wt% sodium acrylate, with 100 mM NaOH under irradiation of LED@400 nm; (a, b1) in the set electric field direction (anode \rightarrow cathode: left \rightarrow right), and (b2) in the reversed electric field direction (cathode \rightarrow anode: left \rightarrow right). (Voltage = 30 V); (naringin: 0.5 wt%; lod: 2 wt%)

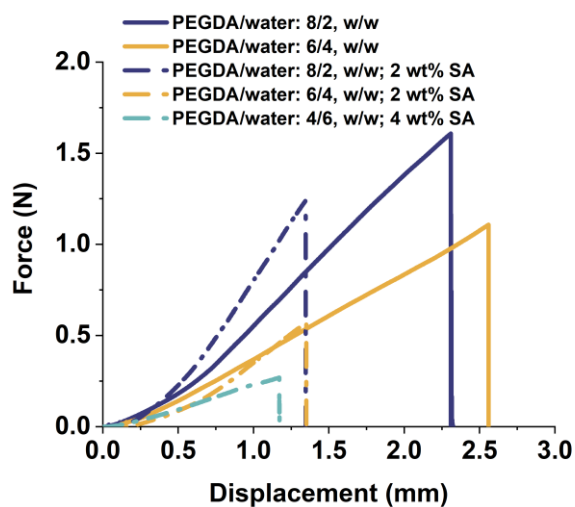


Figure S3.5. Three-point-bend test loading results of a strip structure (20 mm × 3 mm × 2 mm, L × W × H): PEGDA 700/DI water (8/2, w/w), PEGDA 700/DI water (8/2, w/w) in the presence of 2 wt% sodium acrylate, PEGDA 700/DI water (6/4, w/w) in the absence and the presence of 2 wt% sodium acrylate, and PEGDA 700/DI water (4/6, w/w) in the presence of 4 wt% sodium acrylate with 100 mM NaOH.

Chapter 4 Ellagic acid: a natural photoinitiator extracted from pomegranate for the 3D printing application of smart switch

4.1 Preface

Flavone derivatives have been investigated as photoinitiators for both hydrophobic and hydrophilic light-sensitive formulations in the previous chapters. Alternatively, this chapter introduces a natural polyphenol, ellagic acid, to expand the scope of natural photoinitiators. Ellagic acid is abundant in pomegranate, nuts, etc.¹ and has add-on effects on several diseases.¹ With the knowledge of its therapeutic properties, ellagic acid is biocompatible. In the present chapter, to achieve the aforementioned objectives in introduction chapter, the photophysical properties of ellagic acid and the photochemical reactions between ellagic acid and a selected coinitiator have been unraveled. Meanwhile, its photoinitiation ability under visible-light irradiation has been evaluated in PEGDA formulations under mild LED@400 nm. Furthermore, its potential for 3D resin has been validated by a successful 3D printed figurine, and an advanced application, smart switch, has been fabricated using ellagic acid-based 3D resin and achieved upon the contact of water.

4.2 Abstract

Hydrogel devices have been emerging in recent years due to their ability to undergo significant volumetric change in response to environmental conditions. However, the conventional manufacturing methods confine the possibility of highly customized hydrogel devices on request. In this regard, photopolymerization-based 3D printing technique can meet the requirements thanks to its temporospatial control capability. Nevertheless, the active component in 3D ink, photoinitiator, lacks safety assessment that can minimize environmental and health concerns. To address this issue, we develop a pomegranate-extracted polyphenol, ellagic acid, as a biocompatible photoinitiator for free radical photopolymerization of poly(ethylene glycol) diacrylate. As evidence of 3D printability, a high-fidelity 3D printed Gandalf figurine is obtained with detailed facial textures. Additionally, based on the conceptual model of a bilayer hydrogel, two ellagic acid-based 3D inks are involved in a multi-material 3D printing process. The fabricated bilayer hydrogel demonstrates its water-sensitive curling behavior and the airdrying induced reverse recovery. Furthermore, a bilayer smart switch is assembled with an origami room and door. The 3D-printed smart switch is altered to an “open” state upon water contact.

4.3 Introduction

With the increasing demands for lifestyle regulation and fitness records, a growing market for smart devices has emerged and evolved in recent years.²⁻⁷ For instance, smart thermometers, barometers, humidity meters, smart appliances, and wearable medical devices, etc.⁸⁻¹³ However, unexpected circumstances, for instance, flooding, may temporarily disable or permanently damage those devices and obtain unreliable data. Therefore, smart devices must initiate self-protection processes upon the contact of water to avoid potential damage. In this regard, as previously reported,¹⁴⁻¹⁸ with the help of responsive polymers, the self-protection could be achieved upon corresponding stimuli such as water. Specifically, when a water-stimulated shape memory polymer was integrated in an electricity circuit,¹⁶ the introduction of water can initiate shape transformation, thus manipulating on-off states of the circuit. Typically, upon the contact of water, the polymer bent and induced an open-circuit state, i.e., power cut. Conversely, with the decreased water content, the polymer straightened up again and induced a closed-circuit state. In another scenario, greenhouse water collection systems may also require a smart switch during rainfall. Based on the structure of the water collection module,¹⁹ the additional cap integrated with a smart switch can facilitate the warm-up of the inner temperature without undesired heat exchange. Upon rainfall, the intelligent switch can open the cap, enabling rainwater to flow through the water collector.

Considering the prerequisite size and accurate manufacturing of desirable water-driven switches in precision instruments, controlled manufacture of the resulting parts is crucial. Thanks to the intrinsic capabilities of temporal and spatial control abilities and manufacturing versatile and multi-functional products,²⁰ photopolymerization is a promising technology for the production of smart fine parts.²¹ For instance, using photopolymerization technology, a humidity-responsive biomimetic smart material has been developed and produced recently.²² This earthworm-inspired smart material can loosen soil in rainy conditions, improving rain diffusion. Furthermore, incorporating 3D printing technology, photopolymerization could afford well designed production. However, even though the organic solvent impact on environment and health²³ was eliminated owing to the inherent non-solvent conditions of photopolymerization,²⁴ the used photoinitiator in the study was 2-hydroxy-4'-(2-hydroxyethoxy)-2-methylpropiophenone (Irgacure 2959), of which the migration delivers itself from terrestrial and aquatic compartments due to its water solubility, causing environmental concerns. Specifically, the migrated Irgacure 2595 demonstrates moderate ecotoxicity to algae.²⁵ Similarly, 3D printed smart switches and greenhouse water collectors using photocurable 3D resins either directly or indirectly impact the environment and human health.

Specifically, solvent-soaked humidity-responsive smart switches accelerate the soluble small molecules (i.e., photoinitiators) migration; the watering rains that pass through the greenhouse water collector may extract undesired components on or from collector parts, bringing them into soil planting edible vegetables. Because the migrated commercial photoinitiator notifications have been issued by Rapid Alert System for Food and Feed since 2000,²⁶ it is therefore the biocompatibility and environmental impact of photoinitiators should be carefully considered when developing a photoinitiator for smart switches, despite its catalytic amount.

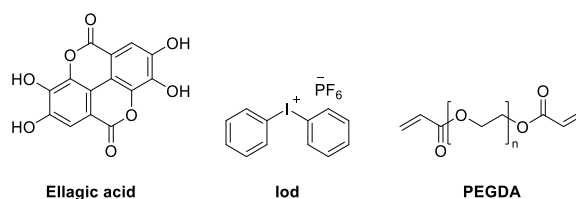
To develop favorable photoinitiators, the exploration and the development of natural candidates are imperative. Many naturally occurring compounds have been investigated as efficient alternatives such as riboflavin, curcumin, flavones, chlorophyll, etc.²⁷⁻³⁴ Because of their natural origins, they exhibited no harm to the environment. Meanwhile, the abovementioned natural photoinitiators demonstrated excellent biocompatibilities and fair photoinitiation abilities. For example, riboflavin can initiate photopolymerization for the fabrication of bone regeneration scaffold under irradiation of violet-blue light.³⁴ The resultant scaffold demonstrated exceptional biocompatibility in terms of cell viability and cell proliferation, etc.³⁴ However, the used light intensity was extremely high (2100 mW cm^{-2}), thus leading to unfavorable energy efficiency. Besides, the intense light is also harmful to retina.³⁵⁻³⁸ In addition, the photoinitiation ability under only intense light limits its application to desktop digital light processing (DLP) 3D printers, as the light intensity of the integrated projector is usually less than 20 mW cm^{-2} .³⁹⁻⁴⁴ As smart switches should be aligned with the designed structure of target objects with the help of photopolymerization-based 3D printing technique, the 3D printability of photocurable resins must be considered. Therefore, a naturally occurring compound exhibiting excellent photoinitiation ability under mild irradiation is anticipated. In this regard, indigo carmine, a plant extract, meets the abovementioned requirements.⁴⁰ Indigo carmine contained 3D resin afforded a 2D-3D reversible hydrogel via photopolymerization-based 3D printing. However, even though indigo carmine is originally a natural dye, it is synthetic in recent decades.⁴⁵ The synthetic process would produce hazard substances to environment. Therefore, the exploration of another naturally occurring photoinitiator candidate draws extensive interest. Moreover, the shape morphing hydrogel was fabricated by a single material and programmed by solely the design of 3D model in the study on the indigo carmine based photoinitiating system.⁴⁰ Contrarily, with the multi-material instead of single material system, the smart hydrogels are expected to be delicately programmed. Therefore, the multi-material 3D resins for programmed smart switches are desirable to expand the application scope of the 3D printed materials.

The present work, therefore, introduces a pomegranate extract, ellagic acid, exhibiting bioactivities thanks to its polyphenol structure (Scheme 4.1).^{1, 46} Due to its neuroprotective activity and natural origin, ellagic acid is a promising safe and environmentally friendly photoinitiator candidate. With the involvement of ellagic acid, the fabrication of hydrogels has the potential for safety-required applications. Furthermore, thanks to the inherent water uptake capabilities of hydrogel, water-stimulated shape morphing was achieved for the development of a water-responsive smart switch. With the existence of water, the water solubility of photoinitiator candidates must be considered. Considering the trivial water solubility and the multi-phenol-hydroxyl groups of ellagic acid, the addition of alkali can improve its water solubility. To investigate its potential as a photoinitiator, its light absorption, steady-state photolysis, and generated radicals were investigated. Thereafter, the formula screening and optimization in terms of their double bond conversions and rates of photopolymerization were conducted. A figurine was then 3D printed to confirm the 3D printability of the developed formula. Furthermore, to program the shape morphing, a multi-material bilayer 3D-printed switch was designed and successfully fabricated. Its function as a smart switch in a water-rich environment was also demonstrated.

4.4 Experimental

4.4.1 Materials

Ellagic acid, diphenyliodonium hexafluorophosphate (Iod), poly(ethylene glycol) diacrylate (PEGDA) M_n 700 and M_n 575, and phenyl-*N*-tert-butyl nitron (PBN) were obtained from Sigma Aldrich and used as delivered. The chemical structures of ellagic acid, Iod, and PEGDA were summarized in Scheme 4.1.



Scheme 4.1. Chemical structures of ellagic acid, Iod, and PEGDA.

4.4.2 Light absorption and steady-state photolysis

The ultraviolet-visible light (UV-vis) absorption properties of ellagic acid in aqueous solutions of NaOH were measured using Varian Cary 50 Bio UV-visible (UV-vis) spectrophotometer from Agilent Technologies. The steady-state photolysis experiments of aqueous solutions of ellagic

acid in the presence of NaOH under irradiation of LED@400 nm (6.4 mW cm⁻²) in the presence of Iod were recorded using the UV-vis spectrophotometer at different irradiation time.

4.4.3 Electron paramagnetic resonance spin trapping (EPR-ST) technique

The free radicals generated from photoreaction between ellagic acid and Iod were characterized by electron paramagnetic resonance spin trapping (EPR-ST) experiments using Bruker E500 spectrometer equipped with a Bruker ER4122 SHQ resonator, as previously reported.³⁰ Briefly, standard X-band EPR tubes of 2.8 mm i.d. containing tert-butylbenzene solution of ellagic acid/Iod was irradiated by LED@400 nm (6.4 mW cm⁻²). The radicals were generated in a nitrogen atmosphere under irradiation and trapped by phenyl-*N*-tert-butyl nitron (PBN) forming PBN/radical adducts, the unique hyperfine splitting constants of which can characterize the trapped radicals. The simulation was processed via the WINSIM application.

4.4.4 Photopolymerization kinetics

The photoinitiation ability of ellagic acid was evaluated via photopolymerization of PEGDA, as previously reported.⁴⁰ Briefly, photopolymerization was monitored using INVENIO®R, Fourier-transform infrared spectroscopy (FTIR) from Bruker. The evenly spread samples between two polypropylene films were placed in FTIR under irradiation of LED@400 nm (6.4 mW cm⁻²). The conversions of PEGDA/water blends were calculated by $D.C. = (1 - \frac{[C=C]_{t=t}}{[C=C]_{t=0}}) = (1 - \frac{\int O.D.d\tilde{\nu}|_{t=t}}{\int O.D.d\tilde{\nu}|_{t=0}}) \times 100\%$. (O.D.: absorbance; $\tilde{\nu}$: wavenumber.), following the decrease of the C-H bond in-plane bending absorbance at 1414 cm⁻¹.^{47, 48} The maximum rates of polymerization ($\frac{dD.C.}{dt} \times 100 = -\frac{1}{[C=C]_{t=0}} \frac{d[C=C]_{t=t}}{dt} \times 100, s^{-1}$) follows the maximum of the first derivative of the double bond conversions versus time curves during photopolymerization. It is important to note that heat release may occur during the sample preparation process, and spontaneous curing may be observed in this rapid formulation. Therefore, it is crucial to add components slowly and carefully.

4.4.5 Swelling kinetics

The cylindrical specimens were produced using a 12 mm diameter and 2 mm height mold and the prepolymers were cured with LED@400 nm irradiation. The weights of the specimens were recorded before they were fully soaked in deionized water. The swollen weights were recorded at 10 min, 20 min, 30 min, 1 hr, 2 hrs, 3 hrs, 4 hrs, and 5 hrs. The swelling uptake (%) was calculated as previously reported⁴⁹ using the following equation:

$$\text{Swelling uptake}(\%) = \frac{m_t - m_0}{m_0} \times 100\%$$

4.4.6 Photorheology

In situ photorheology was carried out using an Anton Paar MCR 702 multidrive rheometer, as previously reported.⁴⁰ Briefly, the sample was set in parallel plate mode (PP25) at a gap of 0.3 mm. The experiment was carried out at constant temperature (25 °C), normal force (0 N), shear strain (0.1%), and frequency (1 Hz). The LED@400 nm (6.4 mW cm⁻²) placed under the sample was switched on after system stabilization. The changes in the moduli of the investigated formulas during photopolymerization were measured as a function of irradiation time.

4.4.7 Three-point bending tests

Measurements of deformation were carried out with an Imada digital force gauge (ZTA-50N). The compression speed was 0.5 mm/min. The specimen was 20 mm × 3 mm × 2 mm (L × W × H) in dimensions, and the distance between contact points was 8.2 mm.

4.4.8 3D printing

The 3D printer (MAKEX) with a LED@405 nm (3 mW cm⁻²) was used for the 3D printing experiments. The 3D resin was premixed thoroughly affording a homogeneous solution under ambient conditions before being loaded into the printer vat.

4.5 Results and Discussion

4.5.1 Photophysical properties and photochemical reactions

Ellagic acid in alkaline solutions demonstrated its visible light absorption from violet to blue-green light, specifically from 400 nm to 500 nm in aqueous solution of sufficient NaOH (Figure 4.1a). Specifically, in the presence of 1 mM NaOH, ellagic acid demonstrated little visible light absorption in visible light range. With the addition of NaOH, the light absorption of ellagic acid at 400 nm increased until the concentration of NaOH reached 100 mM, suggesting the potential of ellagic acid for commercial digital light processing (DLP) 3D printing because most integrated projectors emit light centered at 405 nm. Meanwhile, the maximum absorption of ellagic acid in 100 mM and 500 mM exhibited at 425 nm (Figure 4.1a). The light absorption at 425 nm is assigned to the ring-opened lactone product following deprotonation due to the introduction of NaOH.^{50, 51} Therefore, it was assumed that with the further increase concentration of NaOH, the ring-opening product of ellagic acid was decomposed, resulting in

the decrease of light absorption at 425 nm in 500 mM aq. NaOH. Furthermore, its absorption at 425 nm was an indicative peak for the following studies of its steady-state photolysis in 100 mM and 500 mM aq. NaOH, while 355 nm and 420 nm were the indicative absorption for ellagic acid in 1 mM and 10 mM aq. NaOH respectively (Figure S4.1). With the presence of diphenyliodonium hexafluorophosphate (Iod), the absorption decreases were observed at its light absorption maxima (Figure S4.1). An isosbestic point appeared only in 1 mM aq. NaOH, suggesting single-step photoreactions between ellagic acid and Iod occurred because only starting material and product absorbing species were observed (Figure S4.1a).⁵² However, in more concentrated aq. NaOH (more than 10 mM), multi-step photoreactions happened between ellagic acid and Iod (Figures S1b-d).⁵² In addition, at the abovementioned indicative peaks at 355 nm, 420 nm, and 425 nm, their light absorption decreases under irradiation of LED@400 nm were recorded and grouped (Figure 4.1b). The ellagic acid/Iod combination demonstrated the similar and rapidest photolysis in 100 mM and 500 mM aq. NaOH, suggesting that the further addition of NaOH over 100 mM exhibited limited effect on the photoreaction between ellagic acid and Iod. Consequently, 100 mM was selected as the concentration of NaOH in the following composition of 3D resins, considering its effect and cost-efficiency. With the abovementioned results, a mechanism of photoreactions between ellagic acid and Iod in 100 mM aq. NaOH was proposed. Specifically, upon excitation (Reaction 4.1), the excited ellagic acid interacted with the oxidant, Iod, and a photoproduct was generated from the electron transfer process (Reaction 4.2). To characterize the active photoproducts for the following photoinitiation, an electron paramagnetic resonance spin trapping (EPR-ST) experiment was carried out under irradiation of LED@400 nm (Figure 4.1c). The simulated hyperfine splitting constants ($a_N = 14.3$; $a_H = 2.2$) were assigned to phenyl radical.⁵³ The phenyl radical is the active species that could further initiate free radical photopolymerization of acrylate or methacrylate (Reaction 4.3, Reaction 4.4, and Reaction 4.5).²⁴ Therefore, ellagic acid based photoinitiating system has potential for photoinitiation, and its photoinitiation abilities in the formulas of PEGDA 575 and PEGDA 700 were investigated and discussed in the following section.

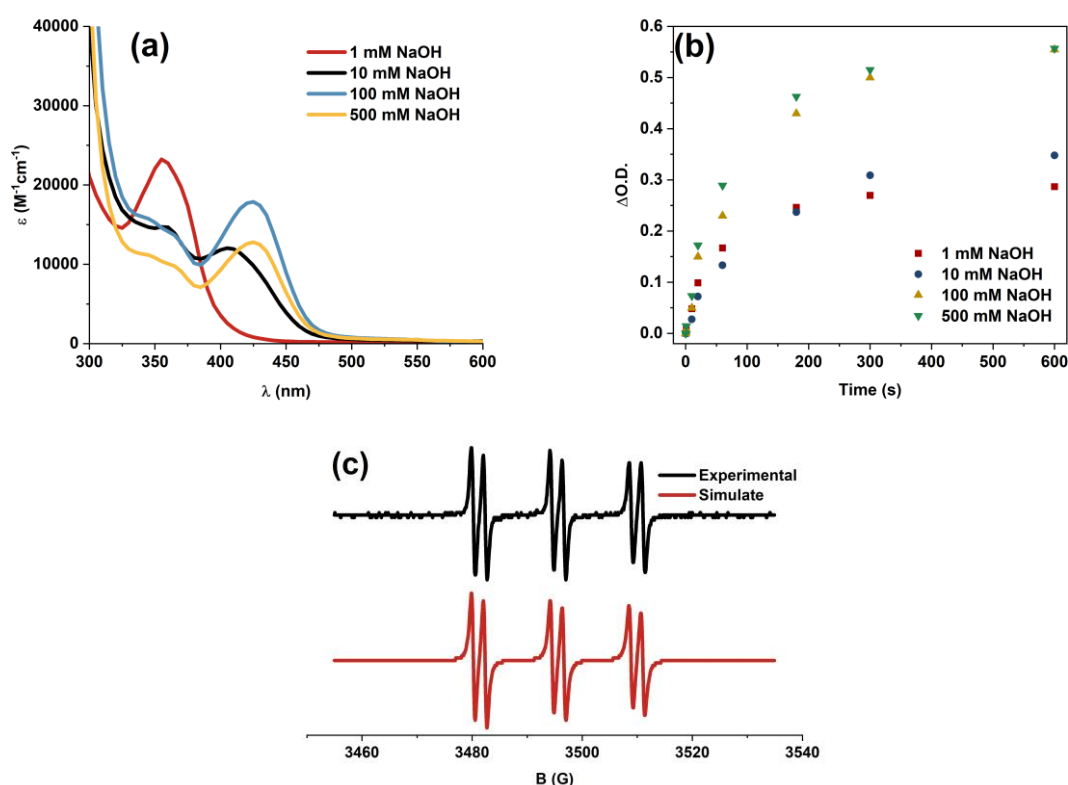
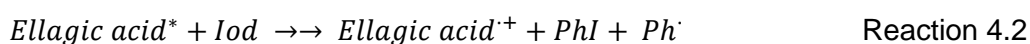


Figure 4.1. (a) UV-vis absorption profiles of ellagic acid in aq. NaOH; (b) O.D. decreases of ellagic acid/Iod (Δ O.D. vs time) at 355 nm in 1 mM aq. NaOH; at 420 nm in 10 mM aq. NaOH; at 425 nm in 100 mM and 500 mM aq. NaOH under irradiation of LED@400 nm; and (c) EPR-ST spectra of the radicals generated in ellagic acid/Iod combination upon exposure to LED@400 nm and trapped by PBN in tert-butylbenzene: PBN/phenyl radical adducts formed in ellagic acid/Iod system: $a_N = 14.3$ G, $a_H = 2.2$ G.⁵³



4.5.2 Photoinitiation ability of ellagic acid and the potential for 3D printing

The study of ellagic acid photoinitiation ability was indispensable for the development of functional 3D resins, and 100 mM was selected as the concentration of NaOH in formulas as aforementioned. Ellagic acid demonstrated excellent photoinitiation abilities for the photopolymerization of poly(ethylene glycol) diacrylate M_n 700 (PEGDA 700) in the presence of 100 mM NaOH under irradiation of LED@400 (Figure 4.2). Specifically, photopolymerization

can occur in the presence of 0.1 wt% ellagic acid (when combined with 2 wt% Iod) which was less than typical concentration of photoinitiators used for photopolymerization (0.5 wt%),⁵⁴ and the final double bond conversion of 45% was observed after 5-min irradiation (Figure 4.2a). With the addition of an extra 0.2 wt% ellagic acid (0.3 wt% in total), the photopolymerization of PEGDA 700 was significantly improved in terms of final double bond conversion (78%). In this regard, the concentration of ellagic acid dominated the manifested photoinitiation ability. However, when the concentration of ellagic acid was increased to 0.5 wt%, the photopolymerization of PEGDA 700 was compromised to the conversion of 59%. The excessive ellagic acid is a likely cause of prevention of light penetration, similar to a previously reported photoinitiator indigo carmine demonstrating bright dye color.⁴⁰ Briefly, the photoinitiation ability was hampered by the excessive indigo carmine which caused a translucent or even opaque formula and thus reduction of light penetration. Likewise, in the studied formula, the dark appearance of resins caused by overloaded colored ellagic acid impeded light penetration, thus preventing the excitation of ellagic acid (Reaction 4.1). Subsequently, decelerated electron transfer occurred, thus reducing the generation of active species, i.e., phenyl radicals (Reaction 4.2). Consequently, the photoinitiation was adversely affected due to accumulated abovementioned effect (Reaction 4.3). In addition, with the increase of ellagic acid, the maximum rate of polymerization was accelerated (Figure 4.2b), reaching its plateau at 0.3 wt% ellagic acid. Specifically, the maximum rates of photopolymerization in the presence of 0.3 wt% or 0.5 wt% were 2.0 s^{-1} , while it was only 1.3 s^{-1} in the formula containing 0.1 wt% ellagic acid. Therefore, 0.3 wt% was selected as the concentration of ellagic acid in formulas for the subsequent studies, considering the resulting double bond conversion and maximum rate of photopolymerization.

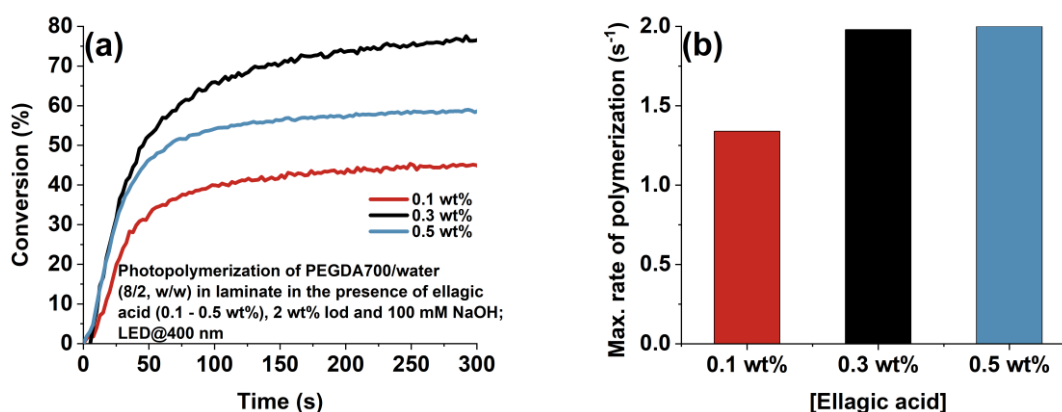


Figure 4.2. (a) Photopolymerization profiles (double bond conversions vs time) of PEGDA 700/water (8/2, w/w) and (b) their maximum rates in laminate in the presence of different concentrations of ellagic acid, 2 wt% Iod, and 100 mM NaOH upon exposure to LED@400 nm (6.4 mW cm^{-2}).

In addition, water plays an important role in the investigated formulation, as it is indispensable for the formation of hydrogel, and it determines the maximum amount of dissolved ellagic acid. As further increase of water content compromised the photopolymerization of PEGDA 700/water as previously reported,⁴⁰ the reduced water content was subsequently investigated in terms of final double conversion of PEGDA 700/water blends (Figure 4.3a). The final double conversions of the investigated PEGDA 700/water ratios were observed from 74% to 82%, suggesting the limited effect of water on the photopolymerization of PEGDA 700/water. However, the polymerization of PEGDA 700/water (8/0.5, wt) cannot occur using ellagic acid/Iod (0.3%/2%, wt) under irradiation of LED@400 nm due to insufficient water to fully dissolve ellagic acid. The dissolved ellagic acid would be inadequate for photoinitiation, and its excessively suspended particles caused light scattering simultaneously. Furthermore, the reduced conversion of PEGDA with addition of water in PEGDA 700/water (8/2, w/w) blend can be ascribed to the dilution of PEGDA in the whole formula. Despite the superior photopolymerization performance of the PEGDA 700/water (8/1.5, wt) observed in the presence of ellagic acid/Iod (0.3%/2%, wt), the water content had to be further evaluated to optimize the formulation for 3D printing. Specifically, as the introduction of water can also affect the mechanical properties of the resulting polymer, the PEGDA 700/water ratio was further optimized to fulfill the shear storage modulus requirement, ensuring integrity of 3D printed objects during the 3D printing pull-up process.⁵⁵ The in-situ shear storage moduli of the three investigated formulas were recorded (Figure 4.3b). Despite the same storage moduli were observed at the end of photopolymerization, the PEGDA 700/water (8/1, w/w) demonstrated the rapidest ascending storage modulus. Because water is a viscous Newtonian liquid,⁵⁶ the increasing water content led to the increase of viscous portion, thus resulting in latent accumulation of storage moduli (Figure 4.3b). Rapidly ascending shear storage modulus has potential to satisfy interfacial shear strength in a short time, thus shortening printing time. Comprehensively considering the photopolymerization and shear stiffness of the investigated PEGDA 700/water ratios, PEGDA 700/water (8/1, w/w) was selected for the following 3D printing study.

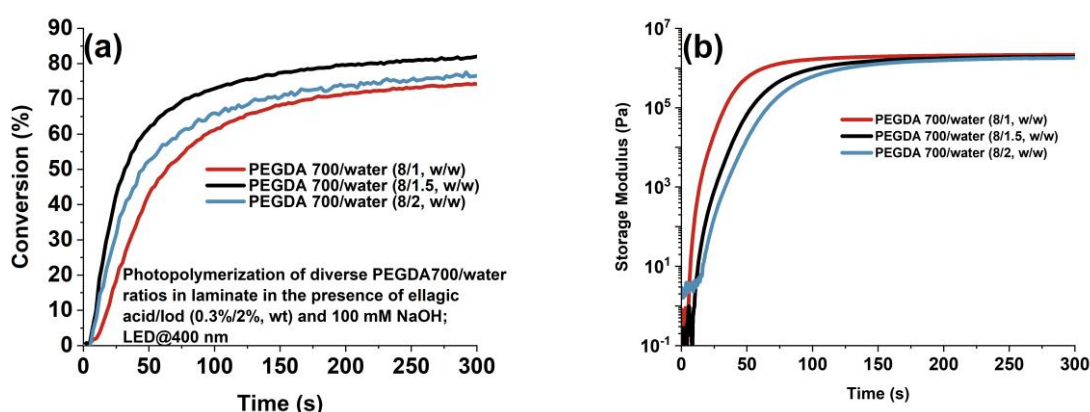


Figure 4.3. (a) Photopolymerization profiles of (double bond conversions vs time) of PEGDA 700/water in diverse ratios and (b) the corresponding in-situ photorheological profiles in the presence of ellagic acid/Iod (0.3%/2%, wt) and 100 mM NaOH upon exposure to LED@400 nm (6.4 mW cm^{-2}).

With the optimized composition of 3D resin, a Gandalf figurine was 3D printed ($9 \times 10 \times 13$ mm, L \times W \times H) using a commercial DLP 3D printer (Figure 4.4). The 3D-printed Gandalf figurine suggested an exceptional 3D printing ability of the designed ellagic acid-employed formula. Specifically, ellagic acid as a photoinitiator afforded detailed facial textures on the 3D-printed Gandalf figurine (Figure 4.4). In contrast, a commercial photoinitiator, phenylbis(2,4,6-trimethylbenzoyl)phosphine oxide (BAPO), induced undesired overcuring during the 3D printing process, thus damaging the 3D printed object, as previously reported.⁵⁷ The overcuring is attributed to the overqualified photoinitiation ability of BAPO and its transparent appearance in the prepared 3D resin which allows maximum light penetration. Thanks to the dark appearance of the ellagic acid-based 3D resin, the effect of light divergence was minimized, and high-fidelity 3D printing was thus observed. Comprehensively, ellagic acid demonstrated its dual roles as a photoinitiator and a photoabsorber for 3D printing simultaneously. Its dual roles can endow ellagic acid-based 3D resins with remarkable 3D printability. Furthermore, the layered curing time of the 3D printing was 10 seconds, thanks to the rapidly ascending shear storage modulus (Figure 4.3b). With high-fidelity and rapid 3D printing, the developed 3D resin had the potential for rapid manufacturing of fine parts via multi-material 3D printing technique.



Figure 4.4. The 3D printed Gandalf figurine using the PEGDA 700/water (8/1, w/w) in the presence of ellagic acid/Iod (0.3%/2%, wt) and 100 mM NaOH. (9 × 10 × 13 mm, L × W × H; layered exposure time: 10 s)

4.5.3 Development of a smart switch

With the emergence and evolution of smart devices, the smart component has garnered significant interest due to its ability to respond immediately to changes in the external environment. For instance, upon appearance of water in the form of flood, rain, and so forth, a smart switch involved in smart devices is responsible for on-off or open-close state transformation to minimize the compromising effects of such unforeseen environmental changes. In this regard, a switch should run an immediate response (e.g., shape transformation) upon water. To fulfill the requirements of switch deformation, the diverse swelling abilities are essential for a bilayer polymeric switch.^{43, 58, 59} Specifically, as the two layers attach to each other, the lower-swelling-ratio layer confines the volume change at the interface, thus inducing a passive bending towards the lower-swelling-ratio layer (Figure 4.5a). To form the difference of swelling ratios, an additional photocurable polymer should be employed as the secondary 3D resin. Considering the excellent photoinitiation performance of the developed ellagic acid-based photoinitiating system in PEGDA 700, a shorter-chain PEGDA was involved as the secondary material candidate. Different chain lengths could result in varying mesh sizes, which can affect the water uptake capacity. As proposed, the swelling behaviors of resultant polymers of PEGDA 700 and PEGDA 575 were distinctive (Figure 4.5b). Specifically, throughout the entire water uptake process (Figure 4.5b), the swelling of PEGDA 700 hydrogel was higher than that of PEGDA 575 hydrogel. Typically, the equilibrium swelling ratio of the polymeric PEGDA 700 (55%) was more than that of polymeric PEGDA 575 (34%) (Figure 4.5b). With the significant difference of equilibrium swelling ratios of polymeric PEGDA 700 and polymeric PEGDA 575, the PEGDA 700 hydrogel layer would result in more volumetric increase, potentially causing obvious bending behavior of multi-material bilayer hydrogel due to the anisotropic swelling behavior at the interface (Figure 4.5a). Ideally, the

bending extent of the polymeric PEGDA 700 layer should be greater than that of the polymeric PEGDA 575 layer to support larger deformation of the former, thus the bilayer made of PEGDA 700 and PEGDA 575 could afford a programmed bending behavior as proposed (Figure 4.5a). Therefore, we proposed a bilayer model with PEGDA 700 and PEGDA 575 utilizing the 3D printing technique (Figure 4.5c). With a designed 3D model, the two separate 3D resins were introduced into the 3D printer tank in order. Therefore, a bilayer polymer would then be fabricated (Figure 4.5c).

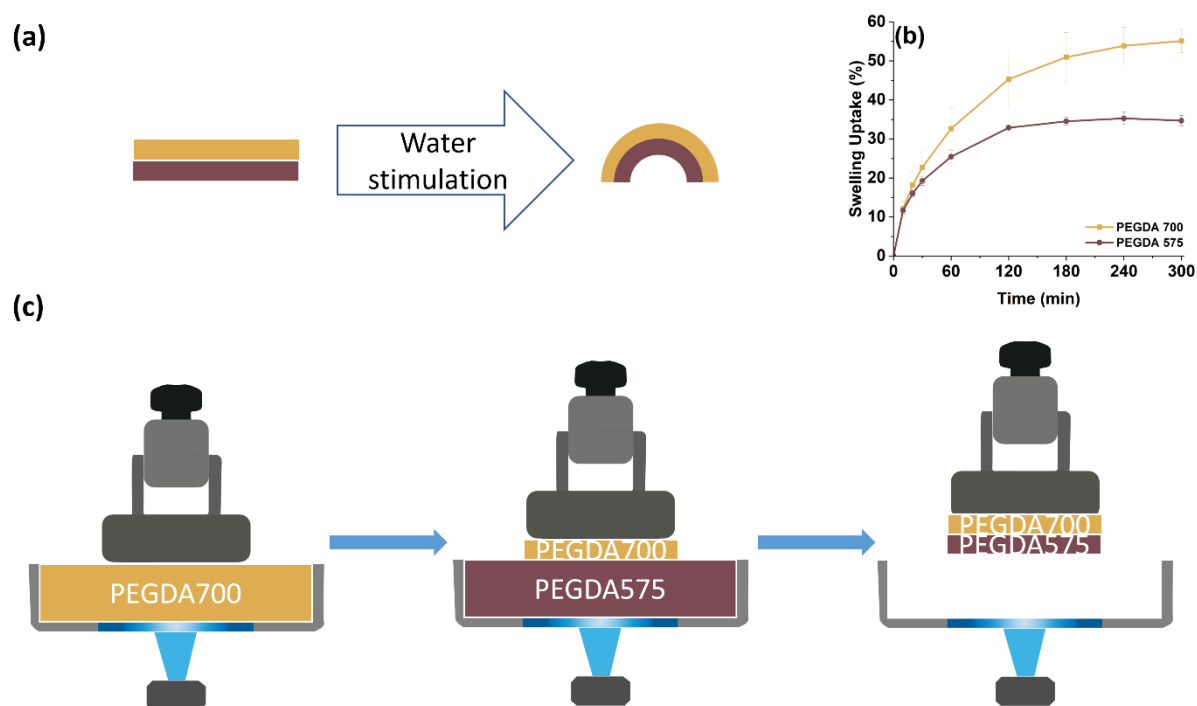


Figure 4.5. (a) Simulated smart hydrogel; (b) swelling kinetics (swelling uptake vs time) of the resultant polymers of PEGDA/water (8/1, w/w) blends in the presence of ellagic acid/Iod (0.3%/2%, wt) and 100 mM NaOH upon exposure to the LED@400 nm (6.4 mW cm^{-2}); and (c) the proposed process of 3D printing.

To validate the abovementioned proposal, additional experiments were involved thereafter using either PEGDA 700/water or PEGDA 575/water blends in the presence of ellagic acid/Iod (0.3%/2%, wt) and 100 mM NaOH. As the interfacial shear storage modulus determines the success of a bottom-up 3D printing, the in situ photorheology study for PEGDA 575/water (8/1, w/w) was performed and compared with PEGDA 700/water (8/1, w/w) (Figure 4.6a). Initially, the higher shear storage modulus of the resin of PEGDA 575/water (8/1, w/w) was observed. This could be ascribed to the suspended particles of residual undissolved ellagic acid, contributing to the elastic modulus, and a similar result was observed previously in a indigo carmine-based photocurable resin.⁴⁰ The two abovementioned polymers of PEGDA 700/water

(8/1 w/w) and PEGDA 575/water (8/1 w/w) were at the same magnitude of final shear storage moduli. The comparable shear storage moduli of the bilayer polymer suggested a uniform in terms of shear stiffness, thus ensuring the integrity of 3D printing. In addition, to estimate the feasibility of the smart hydrogel production, the mechanical strengths in terms of bending were thereafter evaluated to confirm the shape transformation capability, and the results were in line with the proposed bending extents (Figure 4.6b). Specifically, the displacement of PEGDA 700 hydrogel reached 1.7 mm, while that of PEGDA 575 hydrogel was only 1.3 mm (Figure 4.6b). Meanwhile, the polymerized PEGDA 700 could bear larger fracture stress compared to polymerized PEGDA 575 (Figure 4.6b), which supported more water uptake in polymerized PEGDA 700. Comprehensively, the abovementioned results validated the feasibility of the proposed bilayer hydrogel model (Figure 4.5a), and bilayer hydrogel would bend towards polymerized PEGDA 575 in the presence of a water-rich environment because of the larger volume change occurring to polymerized PEGDA 700. Therefore, a multi-material 3D printed smart switch could be achieved.

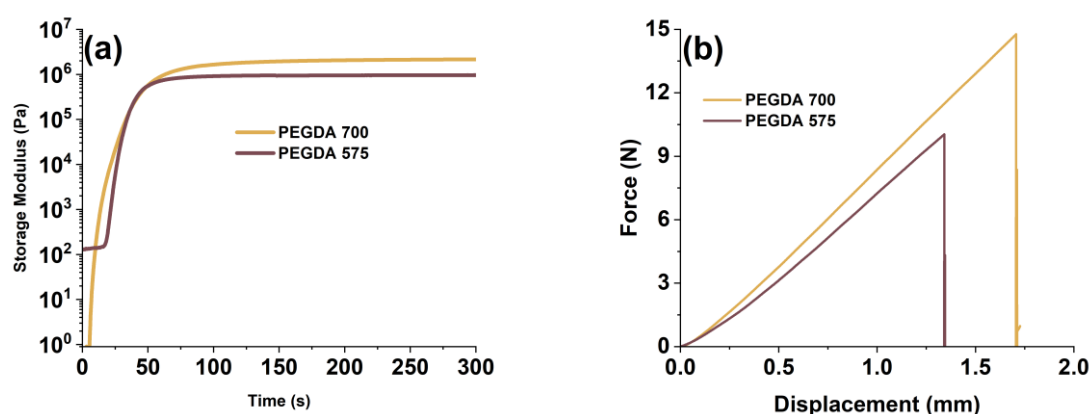


Figure 4.6. (a) In situ photorheology profiles (storage moduli (G') vs time) of PEGDA/water (8/1, w/w) in laminate in the presence of ellagic acid/Iod (0.3%/2%, wt) and 100 mM NaOH upon exposure to the LED@400 nm (6.4 mW cm^{-2}) and (b) three-point bending tests (force vs centered displacement) of the corresponding resultant polymers.

Before the fabrication of the 3D-printed switch, the bending behavior of the produced bilayer hydrogel was confirmed by a simplified model (Figure 4.7A). A planar leaf was 3D printed using PEGDA 700/water (8/1, w/w) (25 layers, 0.5 mm) and PEGDA575/water (8/1, w/w) (25 layers, 0.5 mm) in the presence of ellagic acid/Iod (0.3%/2%, wt) and 100 mM NaOH in order (Figure 4.7A-a). Upon immersion in water, the 3D-printed bilayer leaf immediately curled towards the direction of the polymerized PEGDA 575 layer (Figure 4.7A-b). From both the front (Figure 4.7A-b1) and back (Figure 4.7A-b2) sides, the obvious shadow of the 3D structure was observed, suggesting a “V” shape was formed. The shape transforming behavior suggested a

potential successful smart switch effective upon water contact. Interestingly, under air drying, the curled bilayer hydrogel gradually recovered to its initial state. This phenomenon encouraged the advanced application of the proposed smart switch sensitive to water, and the recovery of the 3D printed leaf indicated the potential recoverability of smart switches.

With the confirmation of the bending behavior occurred to the designed bilayer hydrogel, a smart switch was designed specifically for an origami room. Subsequently, it was successfully 3D printed and assembled as a hinge using PEGDA 700/water (8/1, w/w) (30 layers, 0.6 mm) and PEGDA575/water (8/1, w/w) (30 layers, 0.6 mm), and its transformational response was observed. Initially, the origami door was closed as designed (Figure 4.7B-a). Upon contact with water, the door was opened by the force from the 3D-printed smart switch instantly (Figure 4.7B-b). With 3D printing, we can also design a smart switch specific to desired devices and control the on-off states or open-close states based on assembly directions. With the conceptual design and these results, the developed ellagic acid-based 3D inks were potential for the further smart hydrogel devices in the field of tissue engineering besides smart devices by incorporating selected cells.⁴³

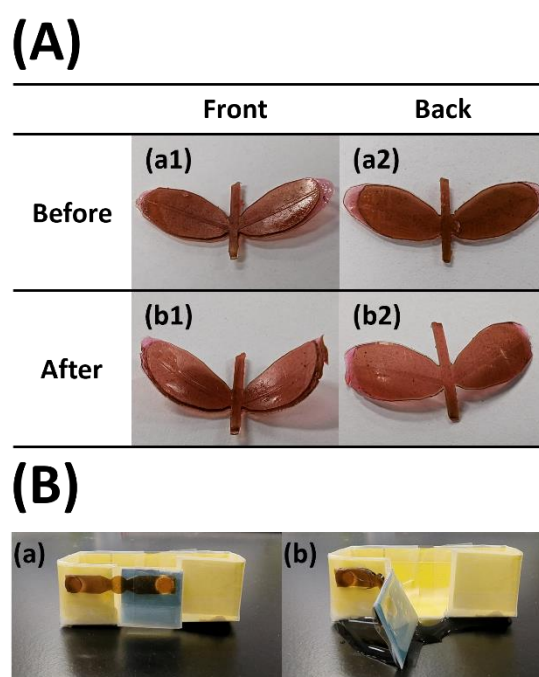


Figure 4.7. (A) The water-driven self-folding assembly process of 3D printed leaves (a) before and (b) after immersion in deionized water for 5 min at ambient temperature at its (1) front and (2) back views; (B) 3D printed water-sensitive smart switch (a) before and (b) after stimulated by deionized water.

4.6 Conclusion

Ellagic acid has demonstrated its excellent photoinitiation ability for PEGDA in the presence of NaOH under a mild LED irradiation, and the preliminary photoreaction mechanism confirmed that the phenyl radical was the active species for the free radical photopolymerization. The effect of the amount of ellagic acid was firstly positive and subsequently negative due to its dark appearance, demonstrating its second role as a photoabsorber for 3D printing. Meanwhile, the optimized water content ensured adequate shear stiffness for the integrity of bottom-up 3D printing. Therefore, with the developed ellagic acid 3D resin, a high-fidelity Gandalf figurine was successfully 3D printed, suggesting the excellent 3D printing ability of the developed 3D resin for further applications. Subsequently, two bilayer polymeric materials were designed and successfully fabricated. Owing to the distinctive swelling ratios and resulting shape transformation capabilities of the two layers, the bilayer polymers demonstrated their programmed responses upon external stimulation of water. In addition, the curled hydrogel can be recovered following an air-drying process. Furthermore, the designed smart switch specifically for an origami room door demonstrated its sensitivity to water and the feasibility of a smart switch. Besides the demonstrated applications, considering the inherent bioactivities, ellagic acid endowed the developed 3D resins with the potential for biomaterials.

4.7 References:

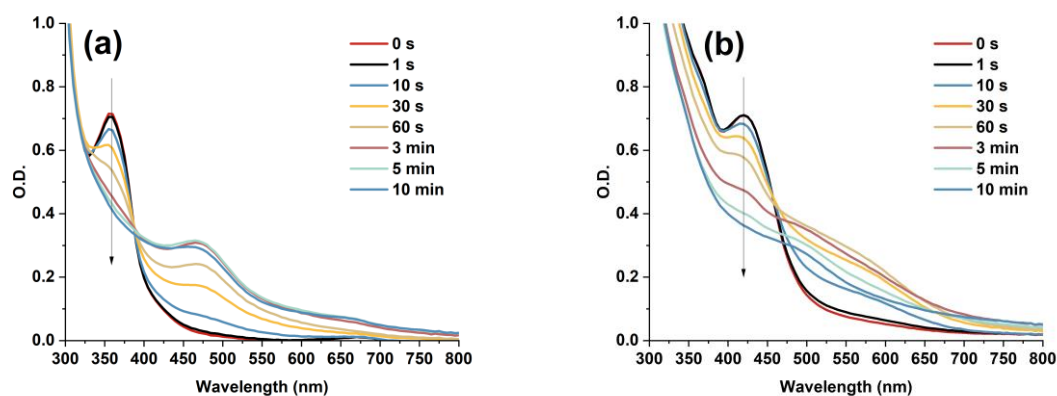
- (1) Alfei, S.; Turrini, F.; Catena, S.; Zunin, P.; Grilli, M.; Pittaluga, A. M.; Boggia, R. Ellagic acid a multi-target bioactive compound for drug discovery in CNS? A narrative review. *Eur. J. Med. Chem.* **2019**, *183*, 111724.
- (2) Zeng, X.; Hu, Y. Sensation and Perception of a Bioinspired Flexible Smart Sensor System. *ACS Nano* **2021**, *15* (6), 9238-9243.
- (3) Muck, J. E.; Unal, B.; Butt, H.; Yetisen, A. K. Market and Patent Analyses of Wearables in Medicine. *Trends Biotechnol.* **2019**, *37* (6), 563-566.
- (4) Shi, X.; Luo, J.; Luo, J.; Li, X.; Han, K.; Li, D.; Cao, X.; Wang, Z. L. Flexible Wood-Based Triboelectric Self-Powered Smart Home System. *ACS Nano* **2022**, *16* (2), 3341-3350.
- (5) Shi, Q.; Zhang, Z.; Yang, Y.; Shan, X.; Salam, B.; Lee, C. Artificial Intelligence of Things (AIoT) Enabled Floor Monitoring System for Smart Home Applications. *ACS Nano* **2021**, *15* (11), 18312-18326.
- (6) Dong, B.; Shi, Q.; Yang, Y.; Wen, F.; Zhang, Z.; Lee, C. Technology evolution from self-powered sensors to AIoT enabled smart homes. *Nano Energy* **2021**, *79*.
- (7) Hao, S.; Jiao, J.; Chen, Y.; Wang, Z. L.; Cao, X. Natural wood-based triboelectric nanogenerator as self-powered sensing for smart homes and floors. *Nano Energy* **2020**, *75*.
- (8) Bariya, M.; Shahpar, Z.; Park, H.; Sun, J.; Jung, Y.; Gao, W.; Nyein, H. Y. Y.; Liaw, T. S.; Tai, L. C.; Ngo, Q. P.; et al. Roll-to-Roll Gravure Printed Electrochemical Sensors for Wearable and Medical Devices. *ACS Nano* **2018**, *12* (7), 6978-6987.
- (9) Khan, Y.; Ostfeld, A. E.; Lochner, C. M.; Pierre, A.; Arias, A. C. Monitoring of Vital Signs with Flexible and Wearable Medical Devices. *Adv. Mater.* **2016**, *28* (22), 4373-4395.

- (10) Long, Y.; Li, J.; Yang, F.; Wang, J.; Wang, X. Wearable and Implantable Electroceuticals for Therapeutic Electrostimulations. *Adv. Sci.* **2021**, *8* (8), 2004023.
- (11) Moon, D. I.; Pleckaityte, G.; Choi, T.; Seol, M. L.; Kim, B.; Lee, D.; Han, J. W.; Meyyappan, M. On-Demand Printing of Wearable Thermotherapy Pad. *Adv. Healthcare Mater.* **2020**, *9* (4), e1901575.
- (12) Park, D. Y.; Joe, D. J.; Kim, D. H.; Park, H.; Han, J. H.; Jeong, C. K.; Park, H.; Park, J. G.; Joung, B.; Lee, K. J. Self-Powered Real-Time Arterial Pulse Monitoring Using Ultrathin Epidermal Piezoelectric Sensors. *Adv. Mater.* **2017**, *29* (37), e1702308.
- (13) Tan, M.; Xu, Y.; Gao, Z.; Yuan, T.; Liu, Q.; Yang, R.; Zhang, B.; Peng, L. Recent Advances in Intelligent Wearable Medical Devices Integrating Biosensing and Drug Delivery. *Adv. Mater.* **2022**, *34* (27), e2108491.
- (14) Zhang, C. L.; Cao, F. H.; Wang, J. L.; Yu, Z. L.; Ge, J.; Lu, Y.; Wang, Z. H.; Yu, S. H. Highly Stimuli-Responsive Au Nanorods/Poly(N-isopropylacrylamide) (PNIPAM) Composite Hydrogel for Smart Switch. *ACS Appl. Mater. Interfaces* **2017**, *9* (29), 24857-24863.
- (15) Zhao, R.; Kang, S.; Wu, C.; Cheng, Z.; Xie, Z.; Liu, Y.; Zhang, D. Designable Electrical/Thermal Coordinated Dual-Regulation Based on Liquid Metal Shape Memory Polymer Foam for Smart Switch. *Adv. Sci.* **2023**, *10* (8), e2205428.
- (16) Yang, H.; Lu, H.; Miao, Y.; Cong, Y.; Ke, Y.; Wang, J.; Yang, H.; Fu, J. Non-swelling, super-tough, self-healing, and multi-responsive hydrogels based on micellar crosslinking for smart switch and shape memory. *Chem. Eng. J.* **2022**, *450*.
- (17) Cai, G.; Ciou, J.-H.; Liu, Y.; Jiang, Y.; Lee, P. S. Leaf-inspired multiresponsive MXene-based actuator for programmable smart devices. *Sci. Adv.* **2019**, *5* (7), eaaw7956.
- (18) Sun, N.; Sun, P.; Wu, A.; Qiao, X.; Lu, F.; Zheng, L. Facile fabrication of thermo/redox responsive hydrogels based on a dual crosslinked matrix for a smart on-off switch. *Soft Matter* **2018**, *14* (21), 4327-4334.
- (19) YONGQUAN, C. Combined greenhouse water collection module. China CN105475044A, 2016.
- (20) Le, X.; Lu, W.; Zhang, J.; Chen, T. Recent Progress in Biomimetic Anisotropic Hydrogel Actuators. *Adv. Sci.* **2019**, *6* (5), 1801584.
- (21) Detamornrat, U.; McAlister, E.; Hutton, A. R. J.; Larraneta, E.; Donnelly, R. F. The Role of 3D Printing Technology in Microengineering of Microneedles. *Small* **2022**, *18* (18), e2106392.
- (22) Yang, Z.; An, Y.; He, Y.; Lian, X.; Wang, Y. A Programmable Actuator as Synthetic Earthworm. *Adv. Mater.* **2023**, *35* (36), e2303805.
- (23) Ridgway, P.; Nixon, T. E.; Leach, J. P. Occupational exposure to organic solvents and long-term nervous system damage detectable by brain imaging, neurophysiology or histopathology. *Food Chem. Toxicol.* **2003**, *41* (2), 153-187.
- (24) Fouassier, J. P. *Photoinitiation, Photopolymerization, and Photocuring: Fundamentals and Applications*; Carl Hanser Verlag GmbH & Co, 1995.
- (25) *National Industrial Chemicals Notification and Assessment Scheme*; NA/991; National Occupational Health and Safety Commission, 2002.
- (26) Aparicio, J. L.; Elizalde, M. Migration of Photoinitiators in Food Packaging: A Review. *Packag. Technol. Sci.* **2015**, *28* (3), 181-203.
- (27) Batchelor, R. R.; Kwandou, G.; Spicer, P. T.; Stenzel, M. H. (-)-Riboflavin (vitamin B2) and flavin mononucleotide as visible light photo initiators in the thiol-ene polymerisation of PEG-based hydrogels. *Polym. Chem.* **2017**, *8* (6), 980-984.
- (28) Encinas, M. V.; Rufs, A. M.; Bertolotti, S.; Previtali, C. M. Free Radical Polymerization Photoinitiated by Riboflavin/Amines. Effect of the Amine Structure. *Macromolecules* **2001**, *34* (9), 2845-2847.
- (29) Zhao, J.; Lalevée, J.; Lu, H.; MacQueen, R.; Kable, S. H.; Schmidt, T. W.; Stenzel, M. H.; Xiao, P. A new role of curcumin: as a multicolor photoinitiator for polymer fabrication under household UV to red LED bulbs. *Polym. Chem.* **2015**, *6* (28), 5053-5061.

- (30) Zhu, D.; Peng, X.; Xiao, P. Penta - Hydroxy Flavones - Based Photoinitiating Systems for Free Radical, Cationic, and Thiol - Ene Polymerization upon Exposure to Mild Blue LEDs. *Macromol. Mater. Eng.* **2021**, 306 (6), 2100059.
- (31) Wu, C.; Shanmugam, S.; Xu, J.; Zhu, J.; Boyer, C. Chlorophyll a crude extract: efficient photo-degradable photocatalyst for PET-RAFT polymerization. *Chem. Commun.* **2017**, 53 (93), 12560-12563.
- (32) Shanmugam, S.; Xu, J.; Boyer, C. Utilizing the electron transfer mechanism of chlorophyll a under light for controlled radical polymerization. *Chem. Sci.* **2015**, 6 (2), 1341-1349.
- (33) Applegate, M. B.; Partlow, B. P.; Coburn, J.; Marelli, B.; Pirie, C.; Pineda, R.; Kaplan, D. L.; Omenetto, F. G. Photocrosslinking of Silk Fibroin Using Riboflavin for Ocular Prostheses. *Adv. Mater.* **2016**, 28 (12), 2417-2420.
- (34) Chang, H. K.; Yang, D. H.; Ha, M. Y.; Kim, H. J.; Kim, C. H.; Kim, S. H.; Choi, J. W.; Chun, H. J. 3D printing of cell-laden visible light curable glycol chitosan bioink for bone tissue engineering. *Carbohydr. Polym.* **2022**, 287, 119328.
- (35) Scorza Barcellona, P.; Campana, A.; Caranti, S.; D'Onofrio, E.; Silvestrini, B. Pretreatment with bendazac attenuates retinal damage induced by intense light in rats. *Pharmacol. Res.* **1991**, 24 (1), 105-112.
- (36) Mainster, M. A. Spectral transmittance of intraocular lenses and retinal damage from intense light sources. *Am. J. Ophthalmol.* **1978**, 85 (2), 167-170.
- (37) Chen, Y.; Perusek, L.; Maeda, A. Autophagy in light-induced retinal damage. *Exp. Eye Res.* **2016**, 144, 64-72.
- (38) Tanito, M.; Kaidzu, S.; Ohira, A.; Anderson, R. E. Topography of retinal damage in light-exposed albino rats. *Exp. Eye Res.* **2008**, 87 (3), 292-295.
- (39) Zhu, D.; Peng, X.; Wagner, P.; Xiao, P. Symmetrically-substituted Thiazolo[5,4-d]thiazole derivatives as both photoinitiators and dyes for 3D printing under violet LED. *Dyes Pigm.* **2022**, 206, 110638.
- (40) Zhu, D.; Peng, X.; Xiao, P. Indigo Carmine: A Base and Neutral Electrolyte-mediated Photoinitiator for 3D Printing in High Fidelity. *Addit. Manuf.* **2022**, 59, 103154.
- (41) Wang, G.; Hill, N. S.; Zhu, D.; Xiao, P.; Coote, M. L.; Stenzel, M. H. Efficient Photoinitiating System Based on Diaminoanthraquinone for 3D Printing of Polymer/Carbon Nanotube Nanocomposites under Visible Light. *ACS Appl. Polym. Mater.* **2019**, 1 (5), 1129-1135.
- (42) Jung, K.; Corrigan, N.; Ciftci, M.; Xu, J.; Seo, S. E.; Hawker, C. J.; Boyer, C. Designing with Light: Advanced 2D, 3D, and 4D Materials. *Adv. Mater.* **2020**, 32 (18), e1903850.
- (43) Kim, S. H.; Seo, Y. B.; Yeon, Y. K.; Lee, Y. J.; Park, H. S.; Sultan, M. T.; Lee, J. M.; Lee, J. S.; Lee, O. J.; Hong, H.; et al. 4D-bioprinted silk hydrogels for tissue engineering. *Biomaterials* **2020**, 260, 120281.
- (44) Moore, D. G.; Barbera, L.; Masania, K.; Studart, A. R. Three-dimensional printing of multicomponent glasses using phase-separating resins. *Nat. Mater.* **2020**, 19 (2), 212-217.
- (45) König, J. Food colour additives of synthetic origin. In *Colour Additives for Foods and Beverages*, Elsevier Ltd., 2015; pp 35-60.
- (46) Peng, R.; Wu, Q.; Chen, J.; Ghosh, R.; Chen, X. Isolation of ellagic acid from pomegranate peel extract by hydrophobic interaction chromatography using graphene oxide grafted cotton fiber adsorbent. *J. Sep. Sci.* **2018**, 41 (3), 747-755.
- (47) Witte, R. P.; Blake, A. J.; Palmer, C.; Kao, W. J. Analysis of poly(ethylene glycol)-diacrylate macromer polymerization within a multicomponent semi-interpenetrating polymer network system. *J. Biomed. Mater. Res., Part A* **2004**, 71 (3), 508-518.
- (48) Silverstein, R. M.; Webster, F. X.; Kiemle, D. J.; Bryce, D. L. *Spectrometric Identification of Organic Compounds*; Wiley, 2014.
- (49) Shin, J. Y.; Yeo, Y. H.; Jeong, J. E.; Park, S. A.; Park, W. H. Dual-crosslinked methylcellulose hydrogels for 3D bioprinting applications. *Carbohydr. Polym.* **2020**, 238, 116192.

- (50) Hasegawa, M.; Terauchi, M.; Kikuchi, Y.; Nakao, A.; Okubo, J.; Yoshinaga, T.; Hiratsuka, H.; Kobayashi, M.; Hoshi, T. Deprotonation Processes of Ellagic Acid in Solution and Solid States. *Monatsh. Chem.* **2003**, *134* (6), 811-821.
- (51) Hostnik, G.; Tosovic, J.; Stumpf, S.; Petek, A.; Bren, U. The influence of pH on UV/Vis spectra of gallic and ellagic acid: A combined experimental and computational study. *Spectrochim. Acta, Part A* **2022**, *267* (2), 120472.
- (52) Kaspar, F. Quality Data from Messy Spectra: How Isometric Points Increase Information Content in Highly Overlapping Spectra. *ChemBioChem* **2023**, *24* (7), e202200744.
- (53) Buettner, G. R. Spin trapping: ESR parameters of spin adducts. *Free Radical Biol. Med.* **1987**, *3* (4), 259-303.
- (54) Zhu, D.; Wagner, P.; Xiao, P. Terthiophene Derivative-Based Photoinitiating Systems for Free Radical and Cationic Polymerization under Blue LEDs. *Ind. Eng. Chem. Res.* **2021**, *60* (24), 8733-8742.
- (55) Levato, R.; Dudaryeva, O.; Garciamendez-Mijares, C. E.; Kirkpatrick, B. E.; Rizzo, R.; Schimelman, J.; Anseth, K. S.; Chen, S.; Zenobi-Wong, M.; Zhang, Y. S. Light-based vat-polymerization bioprinting. *Nat. Rev. Methods Primers* **2023**, *3* (1).
- (56) Wang, S.-Q. *Nonlinear polymer rheology macroscopic phenomenology and molecular foundation*; JohnWiley & Sons, 2017.
- (57) Lai, H.; Zhu, D.; Xiao, P. Yellow Triazine as an Efficient Photoinitiator for Polymerization and 3D Printing under LEDs. *Macromol. Chem. Phys.* **2019**, *220* (18), 1900315.
- (58) Qu, G.; Huang, J.; Li, Z.; Jiang, Y.; Liu, Y.; Chen, K.; Xu, Z.; Zhao, Y.; Gu, G.; Wu, X.; et al. 4D-printed bilayer hydrogel with adjustable bending degree for enteroatmospheric fistula closure. *Mater. Today Bio* **2022**, *16*, 100363.
- (59) Kuang, X.; Roach, D. J.; Wu, J.; Hamel, C. M.; Ding, Z.; Wang, T.; Dunn, M. L.; Qi, H. J. Advances in 4D Printing: Materials and Applications. *Adv. Funct. Mater.* **2019**, *29* (2), 1805290.

4.8 Supporting Information



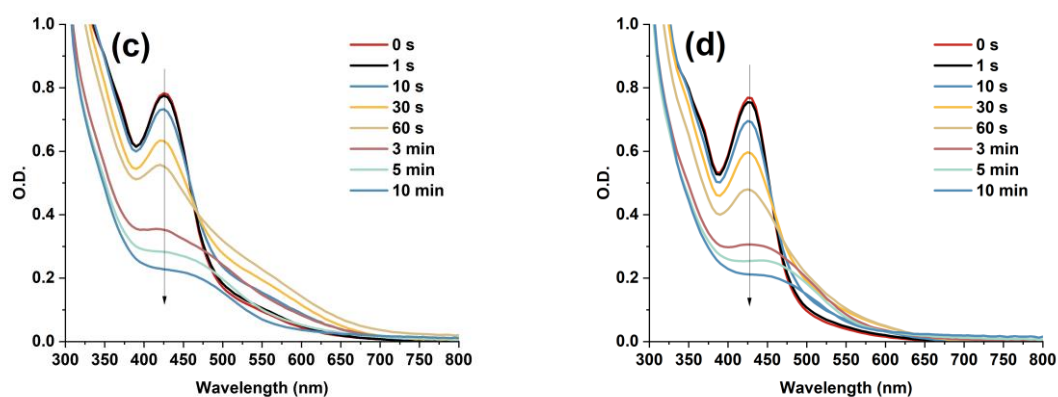


Figure S4.1. The steady-state photolysis of ellagic acid/Iod in (a) 1 mM, (b) 10 mM, (c) 100 mM, and (d) 500 mM aq. NaOH upon exposure to LED@400 nm; UV-vis spectra were recorded at different irradiation times. ($[\text{Iod}] = 4.7 \text{ mM}$)